*Article*

# Assessing the Performance of a Handheld Laser Scanning System for Individual Tree Mapping—A Mixed Forests Showcase in Spain

**Frederico Tupinambá-Simões [1][ID], Adrián Pascual [2], Juan Guerra-Hernández [3,*][ID], Cristóbal Ordóñez [1][ID], Tiago de Conto [2] and Felipe Bravo [1]**

[1] iuFOR, Sustainable Forest Management Research Institute, University of Valladolid, 34004 Palencia, Spain
[2] Department of Geographical Sciences, University of Maryland, College Park, MD 20742, USA
[3] Forest Research Centre, School of Agriculture, University of Lisbon, Tapada da Ajuda, 1349-017 Lisbon, Portugal
[*] Correspondence: juanguerra@isa.ulisboa.pt

**Abstract:** The use of mobile laser scanning to survey forest ecosystems is a promising, scalable technology to describe the 3D structure of forests at a high resolution. We use a structurally complex, mixed-species Mediterranean forest to test the performance of a mobile Handheld Laser Scanning (HLS) system to estimate tree attributes within a forest patch in central Spain. We describe the different stages of the HLS approach: field position, ground data collection, scanning path design, point cloud processing, alignment between detected trees and measured reference trees, and finally, the assessment of main tree structural attributes diameter at breast height (DBH) and tree height considering species and tree size as control factors. We surveyed 418 reference trees to account for omission and commission error rates over a 1 ha plot divided into 16 sections and scanned using two different scanning paths. The HLS-based approach reached a high of 88 and 92% tree detection rate for the best combination of scanning path and point cloud processing modes for the HLS system. The root mean squared errors for DBH estimates varied between species: errors for *Pinus pinaster* were below 2 cm for Scan 02. *Quercus pyrenaica*, and *Alnus glutinosa* showed higher error rates. We observed good agreement between ALS and HLS estimates for tree height, highlighting differences to field measurements. Despite the complexity of the mixed forest area surveyed, our results show that HLS is highly efficient at detecting tree locations, estimating DBH, and supporting tree height measurements as confirmed with airborne laser data used for validation. This study is one of the first HLS-based studies conducted in the Mediterranean mixed forest region, where variability in tree allometries and spacing and the presence of natural regeneration pose challenges for the HLS approach. HLS is a feasible, time-efficient, scalable technology for tree mapping in mixed forests with potential to support forest monitoring programmes such as national forest inventories lacking three-dimensional, remote sensing data to support field measurements.

**Keywords:** precision forestry; terrestrial laser scanning; forest monitoring; mobile laser scanning; forest inventory

## 1. Introduction

The use of Light Detection and Ranging (LiDAR) technology for forest surveying fully supports airborne landscape mapping across many countries, strengthening forest monitoring systems [1,2]. The assimilation of airborne and terrestrial laser scanning data, ALS and TLS, respectively, is solid and expanding towards the collection of super high-resolution point clouds to describe the 3D structure of forests in detail and creating new metrics [3–6]. Forest attributes such as structural complexity are captured from dense point clouds collected with TLS equipment requiring time-consuming operations in the field to produce high-quality 3D point clouds. Scanning a field plot with TLS technology requires

several scans to be merged in post-processing to produce point clouds of homogenous properties [7,8]. The need to make scanning operations faster and cover larger areas has triggered a switch from fixed TLS sensors to mobile TLS sensors capable of generating 3D point clouds collected while on the move [9,10].

Solutions in mobile laser scanners (MLS) have emerged in recent years focusing on maintaining point cloud quality and shortening data acquisition [2,11,12]. One approach is tracking momentum: the handheld mobile laser scanner (HLS), which consists of a LiDAR sensor, an Inertial Measurement Unit (IMU) and, in some cases, a Global Navigation Satellite System (GNSS) receiver. The latter is progressively being replaced by Simultaneous Localization and Mapping (SLAM) algorithms capable of creating digital 3D scenes without embedded GNSS [11,13–15]. Previous studies show that HLS can perform well and time-efficiently for tree mapping, similar in accuracy to TLS in terms of detection of tree locations and estimation of some tree attributes [2,16,17]. Diameter at breast height (DBH) and tree height are two traditionally measured in tree-level mapping and used to benchmark the results from HLS and TLS scans. Factors such as dense canopy cover, scanning design, mixed phenology and structural complexity of the forests challenge the outcomes of laser-based tree-level inventories [18–20]. Moreover, errors in measured reference data for DBH are small compared to field-based measurement of tree height, bringing more complexity to the assessment of tree height. Moreover, errors in the direct measured reference data, such as DBH, are small compared to the indirect measurement, such as tree heights. Involving factors such as operator measurement error for the algorithm to analyse the heights of co-dominated trees, brings more complexity and factors to the evaluation of tree height detection using HLS systems [6,13,21].

The state of the art in HLS mapping has explored forest sites with reasonably favourable conditions for scanning in terms of horizontal and vertical structure, tree spacing and tree species composition [17,18] (Appendix A, Table A1). In this study, we evaluate the performance of an HLS system in mixed-species, complex Mediterranean forest with irregular and clustered distribution of trees showing high structural and morphological variability. Mixed forests use the space differently, both horizontally and vertically, compared to pure stands and this brings complexity to height growth dynamics, phenology, crown development or root structure among other factors [22–25]. Inter- and intra-species covariance regarding tree allometries (i.e., relations between DBH and tree height) brings complexity to scanning and its calibration to measured reference trees [6,26]. Few studies have evaluated the influence of scanning path and point cloud transformation methods in HLS-based tree mapping [9,16,27,28]. In Mediterranean forests, we found two studies: both tested using just one plot and framed under small designs [16,29]. The complexity of these multi-layered and structurally complex forests in the Mediterranean requires a more thoughtful and broader assessment in the light of the few experiences reported so far. Further evidence over larger monitored sites is needed to account for operational scanning factors, better compare results based on HLS to field measurements [30] and allow the use of co-registering ALS surveys as a support of tree height estimation [6,19,29,31]. The latter is especially important as field height measurements are complex, time-consuming and more prone to measurement errors from occlusion, pointing accuracy, phenology or crown shape, among other factors. Estimating the agreement between HLS and ALS for height mapping is a relevant exercise in the context of modern tree mapping possibilities [6,11]. For instance, HLS data could bring important advances to National Forest Inventories (NFIs) to enforce field measurement protocols and provide point cloud data to users to better account for temporal changes and forest dynamics. With this study we expand the understanding of HLS mapping by considering an under-represented but representative showcase of Mediterranean forests.

Specifically, this work evaluates the HLS approach using two different scanning designs and two data transformation modes for point cloud generation. We used an increasingly popular, open-source forest structural complexity tool to process HLS data and to produce species-specific estimations for tree detection, tree diameter, and tree height, for

which estimates were further validated using co-registered ALS surveys [32]. This study, one of the first conducted over Mediterranean forests, evaluates the HLS-based mapping approach over a 1 ha forest encompassing 418 trees, three tree species of different phenology, and alternative scanning paths and HLS transformation modes for processing modes were tested, with a special focus on point cloud processing descriptions and the sequencing of geospatial operations needed to perform the HLS approach for tree mapping.

## 2. Materials and Methods

### 2.1. Study Area and Tree-Level Inventory Data

The study area is located in Jarandilla de la Vera, in the northern region of Extremadura, Spain. We used a 1 ha marteloscope site divided in 16 squared subplots of 25 m side (Figure 1). Marteloscope plots are used to train students and forestry professionals in forest inventory and mensuration, as trees are labelled, measured and geolocated [33,34]. The experiment was installed in 2021 to promote complex forests (mixed and irregular) as a management strategy in response to climate change and declining biodiversity. The site is a mixed forest composed of three main species. Maritime pine (*Pinus pinaster*—Pp) represents 25% of the population, Oak (*Quercus pyrenaica*—Qp) is 60% and 15% rest is for Black Alder (*Alnus glutinosa*—Ag) trees located along the stream crossing the plot. The training data for this study comprised 433 trees—including trees classified as dead or damaged during reference data collection—whose diameter at breast height (DBH) was greater than 5 cm. Reference measurements were collected on 24–26 May 2021 in leaf-on conditions. We used a 1 mm precision calliper for DBH measurements using two field measurements by tree. The average value was used as DBH. Tree heights were measured with a vertex (Haglöf Vertex Laser Geo 360°). Tree locations were precisely registered using a Total Station (Topcon GTS 220). A summary table of the field data is presented in Table 1, including volume with bark (VCC)—calculated using Spanish National Forest Inventory allometries—for the three main species [35]. To inform on horizontal complexity, we used tree locations, DBH measurements and R package 'spatstat.core' to compute the Clark-Evans (CE) aggregation index for the site and for each of the 16 sections. The mean CE value was 0.78 under no edge-correction and 0.80 with it. Clustering conditions (CE < 1) were observed in 9 of the sections (see Appendix B, Figure A1). The site is a good fit to test HLS under heterogeneous conditions of forest horizontal structure due to variability in CE values, dominance of clustering conditions and presence of three main forest species. Terrain conditions across the 1 ha experiment site vary considerably from sandy soils to patches with small rock formations; the presence of a permanent stream abruptly modifies the orography of the western sections (Figure 2). This mix of geo- and biophysical conditions creates a challenging scenario because it complicates the derivation of digital terrain models (DTM) from laser scanning data (ground estimation). Inaccuracies in ground estimation can impact tree location as well as the performance of the algorithms used to determine DBH and tree height estimates from 3D laser data [19,36,37].

### 2.2. Handheld Laser Scanning (HLS)

The HLS data was collected in early February 2022 using a handheld laser scanner model ZEB-Horizon (GeoSLAM Ltd., Nottingham, UK). This HLS system is equipped with a LiDAR Velodyne VLP-16 sensor, mounted in a spinning head, with 100 m range and accuracy ranging from 1 to 3 cm, vertical angular resolution of 2.0° and horizontal resolution of 0.1–0.4°. The HLS system can capture 300,000 points per second in single return, can scan in double-return mode, and uses SLAM technology in data collection. The toolkit for the scanning operations includes a data-logger connected to the handheld scanner where the optical RGB camera and the LiDAR sensor are set. Activating the HLS system for scanning is straightforward and takes approximately 3 min. After departing from the initial control point, successive ground control points (GCP) must be recorded along the track to support the optimal co-registration of the meshed point cloud in post-processing. The ZEB HLS system recognizes a GCP in post-processing when the scanner stops in the same

position for several seconds. We surveyed a grid of 25 by 25 m that define the sub-plots of a marteloscopio, with 30 possible candidates to be used as GCP. For this we used the total station GTS 220. This grid was supported on two external vertices to the perimeter of the marteloscopio, collected with Global Navigation Satellite System (GNSS) receiver (Topcon Hiper SR), in fixed mode through Networked Transport of RTCM via Internet Protocol (NTRIP) to be able to project point clouds based on HLS to eventually integrate ALS data for validation of tree height.
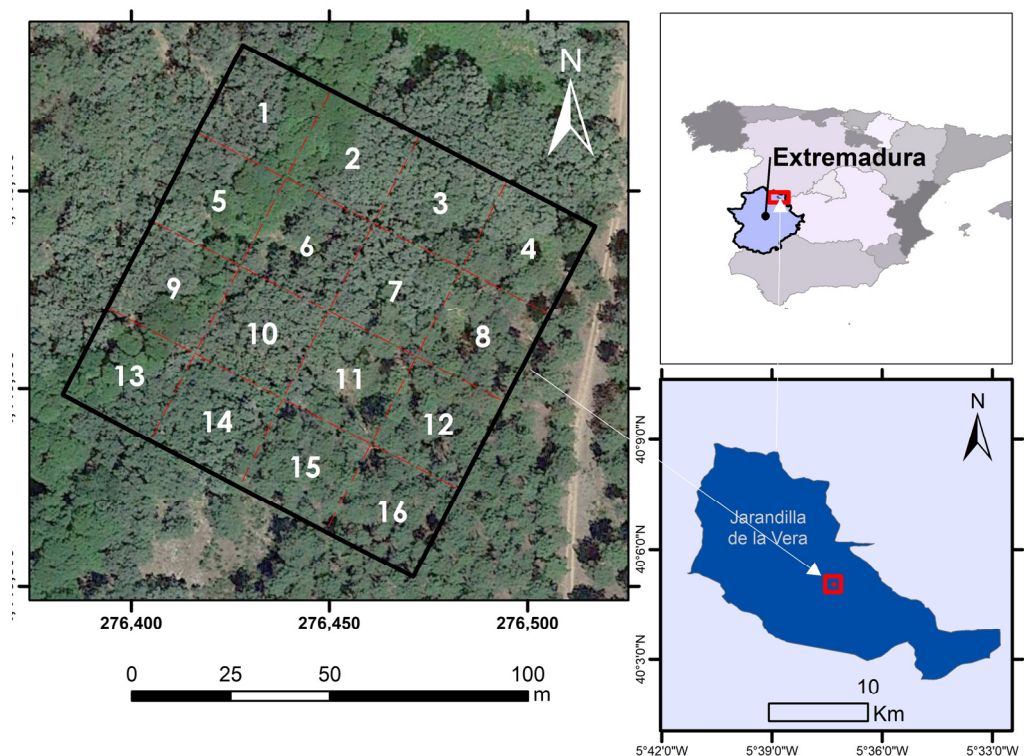


**Figure 1.** Location of the study area in Jarandilla de la Vera, northern region of Extremadura in West Spain. The boundaries of 16 sections conforming the marteloscope (100 m side) are labelled and displayed in light red (left). The background is a drone-based aerial imagery collected during the measuring of tree reference data in leaf-on conditions (25 May 2022). The distribution of black alder (*Alnus glutinosa*) within the site follows, on the western sections, the crossing of the stream along sections 1, 5, 9 and 13.

**Table 1.** Summary of the forest inventory data including tree variables, range and mean values for each of the three species included in the 1 ha marteloscope plot.

| Variable | *Quercus pyrenaica* (Qp) | *Pinus pinaster* (Pp) | *Alnus glutinosa* (Ag) |
|---|---|---|---|
| Number of trees | 257 | 111 | 65 |
| Tree height (H, m) | 4.70–25.80 | 6.70–26.00 | 6.90–26.80 |
| Mean tree height ($H_{mean}$, m) | 16.99 | 21.99 | 21.75 |
| DBH (cm) | 7.05–48.40 | 6.25–65.90 | 18.20–58.15 |
| QMD (cm) | 24.0 | 44.9 | 36.6 |
| Stand basal area (G, $m^2$ $ha^{-1}$) | 11.20 | 17.30 | 6.40 |
| Tree volume (V, $m^3$) | 0.046–1.273 | 0.032–3.20 | 0.074–2.03 |
| Total volume ($m^3$ $ha^{-1}$) | 76.9 | 159.4 | 50.3 |

DBH is Diameter at Breast Height (DBH) and QDM is Quadratic Mean Diameter.
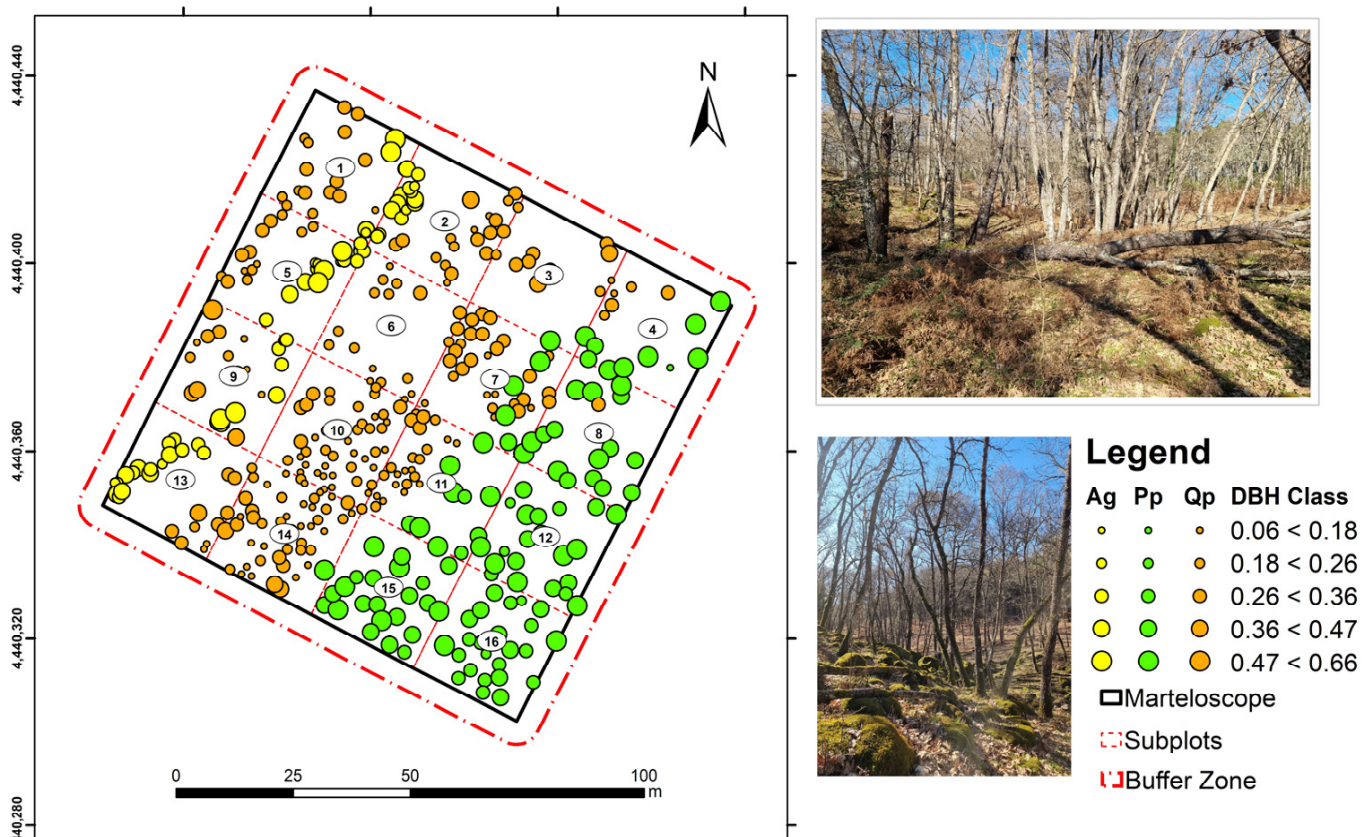
**Figure 2.** Map of the study area showing tree species (yellow: *Alnus glutinosa* (Ag); green: *Pinus pinaster* (Pp); brown: *Quercus pyrenaica* (Qp)) and diameter at breast height (DBH) scaled by symbol size. The perimeter of the marteloscope is outlined in black, and the 16 sub-plots are delimited using red dotted lines. The 5 m external buffer represented with a red dashed-and-dotted line was used to process the laser scanning data.

Two scanning routes were designed to evaluate whether a short, simplified path would render point clouds of similar quality to a more thorough path design to potentially render better results in terms of tree mapping accuracy (Figure 3). Both alternatives started and finished in the same GCP as recommended by the manufacturer. The first scan (Scan 01, 632.4 m) started in the centre of the marteloscope from where HLS data acquisition started towards the NW, then SW and finally back to the origin GCP before replicating the same loop to the eastern sections. Scan 01 transited along 11 CGPs. The second scanning path (Scan 02, 916.8 m) increased its length 50% compared to Scan 01 to have a better coverage of the 16 plot sections. Scan 02 started and ended in the SW corner, the first of the 17 GCPs required along the track. Four GCPs were coincident as forward and backward trajectories matched from the SW reference point. After scanning, the GeoSLAM HUB 6.0 software was used to build the 3D point cloud using coordinates from GCPs surveyed with the total station and transformed to the UTM system. The ZEB HLS system provides two transformation modes for generating the 3D point clouds: the rigid and the none-rigid modes. The characteristics and outcomes of the rigid and none-rigid transformations are further explored in this study.
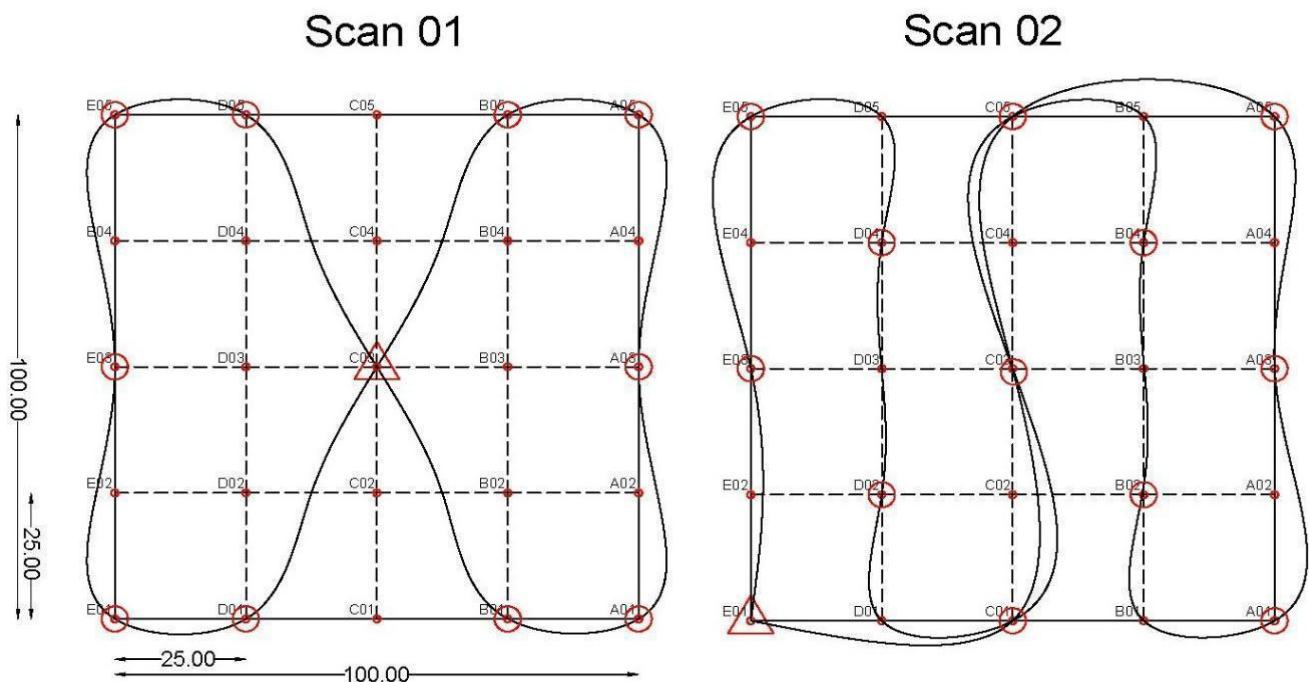
**Figure 3.** Representation of the 100 m × 100 m marteloscope and its 16 sections, each 25 m × 25 m, to show the two scanning paths tested. The red triangle is start-and-end point for each scan, the small red dots represent known points measured with Total Station, and red circles represent the Ground Control Points (GCP) along the scanning and whose positions were later measured using Total Station.

Under the rigid option, the point cloud is rotated and adjusted, and GCP locations are matched without changing the scale factor, i.e., all laser echoes are transformed in one step, and the relative position of points remains invariant. The none-rigid mode does not preserve the relative positions of points, by moving, rotating or changing the scale between points. It is expected to perform better for conditions where SLAM technology better accommodates GCP locations to known GCP coordinates (GeoSLAM Ltd., Nottingham, UK). Hereby, laser points that are closer to the reference points are shifted more than the points that are farther away. Sinuosity in the scanning paths and overlapping along the tracks increase the areas close to GCP for which the switch can affect coordinates values. We explore the effect of transformation mode in this study by processing both Scan 01 and Scan 02 under both options to confirm the expected better performance of the none-rigid mode in terms of consistency in point cloud density, processing time and effects towards the estimation of tree locations and tree attributes.

### 2.3. Point Cloud Post-Processing Using Forest Structural Complexity Tool

The transformed point clouds were exported in LAS format—the standard format for LiDAR data—after masking out the boundaries of the marteloscope using a 5 m buffer to capture edge trees. We used the *lidR* package [38] available in the R statistical software R [39] to filter out laser echoes ranging outside of the buffer. After this step in R, we turned the *Forest Structural Complexity Tool* (FSCT) actionable for t tree mapping. All point clouds created here (2 scans × 2 transformation modes) were not thinned to reduce the dimension of the data. Strategies to reduce the size and density of laser point clouds are well-known [40]—sometimes at the cost of downgrading the data below feasible standards for high-quality tree mapping [41,42]. We compute point cloud density value for the 4 scans across the 16 sections to detect variability in point cloud properties and to better inform on scanning properties (design, transformation mode and length) towards

point cloud properties (density). We have made the four HLS point clouds available (see https://doi.org/10.5281/zenodo.7308680, accessed on 10 December 2022).

FSCT is an open-access point cloud processing solution designed for tree-level forest mapping [43]. Algorithms designed to fast-process 3D data are implemented in FSCT starting from point cloud classification (i.e., laser echoes are classified into vegetation, terrain, and other classes). Laser echoes classified as ground were used to create a digital terrain model and to re-scale the elevation of none-ground laser echoes—common approach in laser-based forest inventory using ALS or TLS [8,43]. Here, point cloud classification and filtering use deep learning to further segment stems from laser echoes initially classified as vegetation. Clustering is then used to segment the skeleton of tree stems and branches: FSCT uses a hierarchical density-based spatial clustering algorithm (HDBSCAN, [44]) before fitting a cylinder-oriented function to derive the longitudinal sections of detected tree stems. The alignment of round-shape sections of tree cylinders and the smoothness of the fitting are some of the operations FCST has automated. The FSCT tool performs a final aggregation of the skeletons to produce single-tree point clouds from which to derive tree positions in a local positioning framework and tree structural attributes including DBH and tree height [17,19,45]. More details on the algorithms involved on each step can be found at https://github.com/SKrisanski/FSCT, accessed on 10 December 2022. We followed the recommended settings by the developers [43]. Tree positions and tree structural outcomes from FSCT were validated using reference trees in the field. As a support, we add integrated Airborne Laser Scanning (ALS) data to enforce the validation of tree height measurements, a frequent source of uncertainty in calibration and validation in forest remote sensing [6].

## 2.4. Airborne Laser Scanning Data for Tree Height Validation

Publicly available ALS data in Spain can be accessed through the National Plan for Aerial Orography (PNOA). The ALS data used in this study is part of the second nationwide round of ALS surveys (for more details about ALS data acquisition in Extremadura North Region, [46]). The ALS data overlapping the 1 ha marteloscope was collected using a RIEGL LMS-Q1560 sensor during leaf-off conditions (January 2019, Figure 4). Although the nominal laser pulse density for the entire region was 2 points per square meter m$^{-1}$, the point cloud density within the boundaries of the marteloscope was substantially higher than the nominal value, with an average of 12.68 points. Shared routines with FSCT were reproduced for ALS data to produce a DTM and use ground-echoes from the ALS to re-scale measurement from ellipsoid to above-ground heights. The normalization process described above was used to produce a canopy height model (CHM) using a raster resolution of 1 m. The processing of ALS data followed standard routines in ALS-based forest inventory [46] using LAStools software [47].

## 2.5. Validation of HLS & FSCT Performance

Reference tree data were used to compare tree positioning, compute tree detection rate, analyse the distribution of omission and commission errors when creating matching tree pairs, and finally, to validate the accuracy of detected estimates for DBH and tree height to ground-truth field measurements. To create a tree matching between a reference tree and a detected tree, several distance thresholds have been proposed in the literature [8,48]. We allowed a maximum distance of 2 m in the two-dimensional space for a detected tree to be a candidate for matching a reference tree. We computed the distance matrix for all measured trees and all possible sets of candidate trees detected. The closest detected tree within a 2 m radius from measured tree coordinates was linked to each measured tree (n = 433). If more than two trees were detected within the 2 m buffer, the candidate tree that minimized the difference in DBH from the measured tree was selected, ensuring one match per measured tree. Important studies from FSCT developers [32] or the reference paper from [8] adopted a similar approach for establishing tree matching pairs.
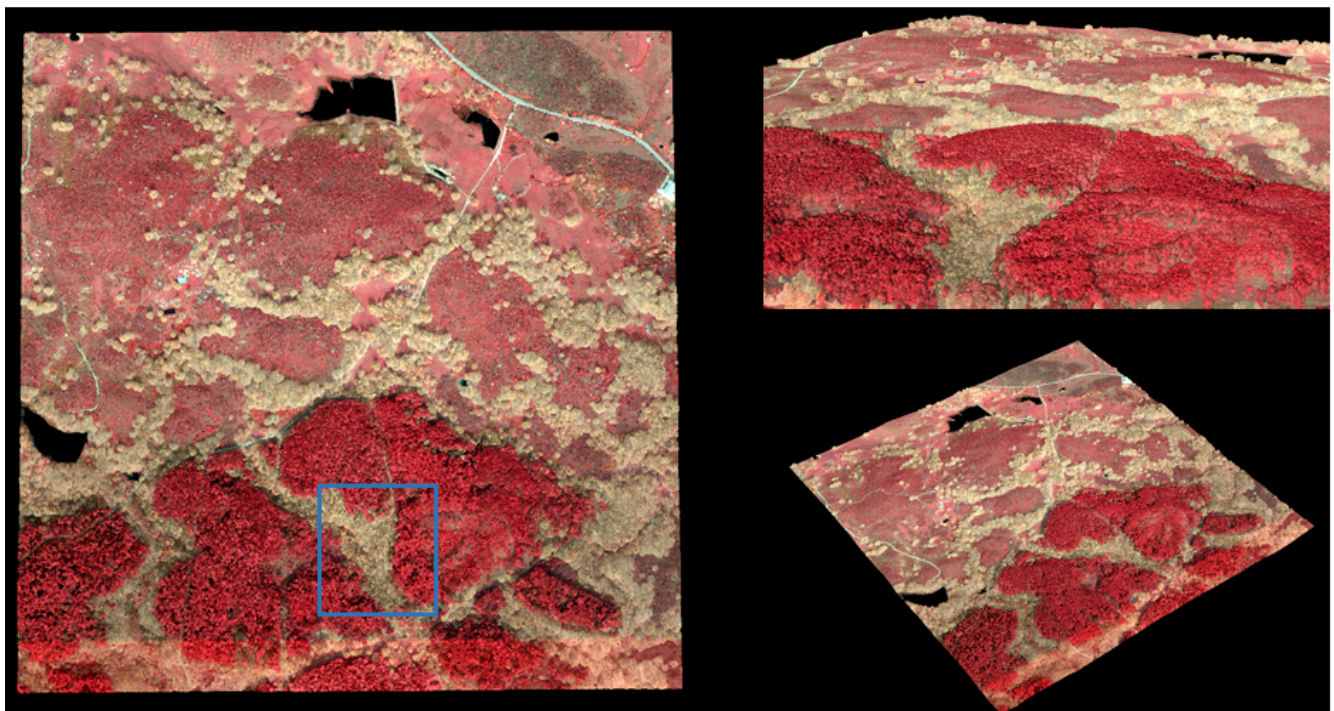
(**a**)
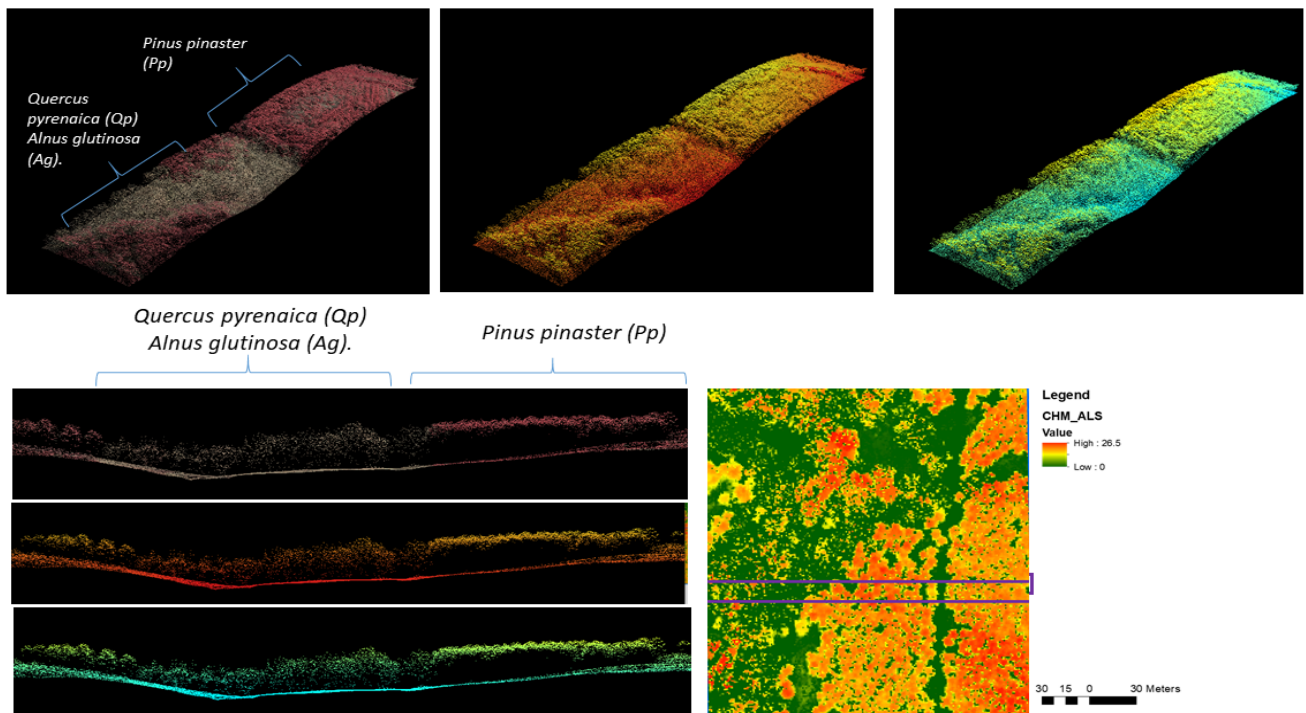


(**b**)

**Figure 4.** The study area (blue boundary) over the ALS data displaying the three main tree species in the study area (**a**). Detailed overview (representing the profiles of infrared, intensity and elevation from ALS point clouds) of the main species represented in the marteloscope and CHM from the study area under leaf-off condition of *Quercus pyrenaica* and *Alnus glutinosa* species (**b**).

The accuracy of tree detection is typically measured using omission and commission errors [8,16,49]. Omission errors account for the proportion of measured trees not detected, while commission errors appear when a detected tree has no matching ground-truth tree under the proposed tree assignment threshold. The 16 sections of the training plot were used as calculation units to relate tree detection rates, and omission and commission error values to site and section specific factors such as tree density, species composition or mean tree size expressed by mean DBH values. The set of matching tree pairs was modelled under simple linear regression model to measure the accuracy of DBH and tree height estimates. Measured referenced data was used as dependent variable and explained by DBH or tree height estimated values. To measure the accuracy of the fit, we used total explained variance ($R^2$), root mean squared error (*RMSE*), relative *RMSE* error expressed over the mean value of the reference data, and similarly for the absolute bias and relative bias:

$$R^2 = 1 - \frac{\sum(y_i - \hat{y}_i)^2}{\sum(y_i - \overline{y_i})^2} \tag{1}$$

$$RMSE = \sqrt{\frac{\sum_{i=1}^{n_s}(y_i - \hat{y}_i)^2}{n_s}} \tag{2}$$

$$Bias = \frac{\sum_{i=1}^{n_s}(y_i - \hat{y}_i)}{n_s} \tag{3}$$

where $n$ is the number of trees of each specie $s$ (3), $y_i$ is the value of DBH or reference tree height $i$ for a detected tree, $\hat{y}_i$ is the value of DBH or tree height for a measured reference tree $i$ in the field and, $\overline{y}_i$ is the predicted value for reference tree $i$ for which there is a detected tree assigned.

The height percentiles from the ALS surveys provide reliable, time-steady canopy height estimates at stand level even in low-density conditions (1–2 points) [1]. Uncertainty from mixed tree phenologies and from the collection of reference tree data during the leaf-on season can be better detected using ALS height stats to further validate field ground truth and HLS data. Canopy crown width measurements and detected coordinates for each matching pair were used to extract ALS echoes co-registering within the 2D space of each tree define by its canopy crown area projected in the ground. Once ALS echoes for each tree were isolated, we computed the maximum elevation of ALS first echoes for each tree. In this way, height measurements collected with the vertex were benchmarked to height estimates from FSCT (HLS data) and from ALS data. To further validate the accuracy of tree height information, we compared tree height estimates from FSCT to the elevation of the coordinates in the HLS data used as input data to run FSCT. This additional step was used to test whether tree heights matched to the maximum elevation of HLS data for each tree region. The research workflow presented in Figure 5 summarizes all steps and processes carried out in this investigation.
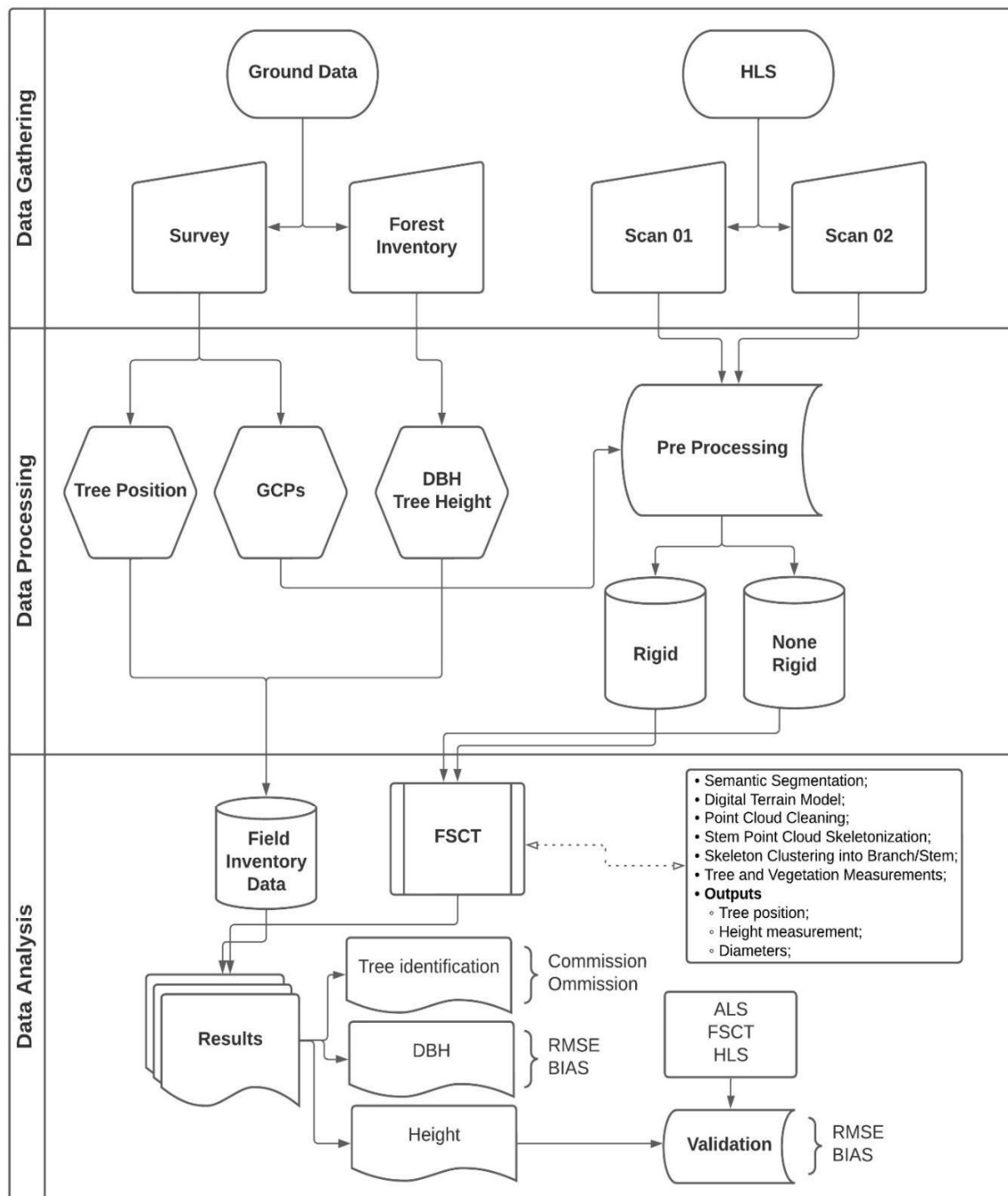
**Figure 5.** Summary of the workflow performed in this research using handheld laser scanning (HLS), the Forest Structural Complexity Tool (FSCT), airborne laser scanning (ALS) to estimate tree detection, diameter at breast height (DBH) and tree height using reference data for calibration.

## 3. Results

### 3.1. Point Cloud Data Pre-Processing

The 1 ha forest was scanned in less than 30 min for the two tested tracks (Table 2). The raw point cloud data comprised almost 200 million laser echoes for Scan 02. Increasing the length of the track by 50% from Scan 01 to Scan 02 had a linear relationship with the increase in computing time. It is worthwhile highlighting the error between point cloud values computed by SLAM and the reference coordinates measured with the Total Station was below 0.5 for Scan 02 while for Scan 01 it reached 2 m under the rigid option available for transformation during the pre-processing. Positioning error was the main difference

between rigid and none-rigid—performing similarly for Scan 02 and diverging in Scan 01 where the none-rigid outperformed the rigid approach by a factor of 8.

**Table 2.** Summary statistics of HLS data collection and computing processing time in the lab using Data from point cloud processing in GeoSLAM software. The reported error informed on the mean difference between measured GCP and the coordinate of each point in the processed point cloud.

| Scan ID | Points (10⁶) | Length (m) | Scan Time | Transform. Method | File Size (Gb) | Processing Time | Trans. Error (m) |
|---------|--------------|------------|-----------|-------------------|----------------|-----------------|------------------|
| Scan 01 | 141.85 | 632.4 | 00:15:57 | Rigid | 1.19 | 00:15:12 | 2.00 |
| | | | | None-Rigid | 1.29 | 00:36:46 | 0.25 |
| Scan 02 | 198.42 | 916.1 | 00:22:23 | Rigid | 1.67 | 00:21:39 | 0.47 |
| | | | | None-Rigid | 1.74 | 00:47:24 | 0.36 |

*3.2. Consistency in Point Cloud Density*

Mean density values for the four alternatives were computed for each section and for the total 1 ha experiment (Table 3). The scanning density in Scan 01 was around 7000 points/m$^2$ and the difference between both transformation modes was around 500 points on average. The better spatial coverage and increment in time (7 min more) and length (300 m more) in Scan 02 compare to Scan 01 resulted in two 3D point clouds of more than 11,000 points/m$^2$ across the site. The standard deviation in Scan 02 was also greater than in Scan 01. Values for each section were mapped together with omission and commission errors to better understand the relation between low densities and the accuracy of the HLS sensor (see Appendix A).

**Table 3.** Mean and standard deviation (SD) of HLS point cloud density (expressed in point per m$^2$) for each of the four scans tested (Scan 01 and Scan 02 under the rigid and none-rigid transformation mode, respectively).

| Subplot | Scan 01 | | Scan 02 | |
|---------|---------|---------|---------|---------|
| | None-Rigid | Rigid | None-Rigid | Rigid |
| Mean | 7179.09 | 6680.26 | 11,184.15 | 11,175.00 |
| SD | 1818.21 | 1905.85 | 2519.52 | 2586.24 |

*3.3. Omission and Commission Errors*

The best correspondence between the set of point clouds assessed and reference data in terms of tree detection (Figure 6, Table 4) was Scan 02 under the rigid mode (412 detected trees), close to the number of reference trees (433 trees). Tree detection rate for Scan was near 90% for both cases, while for Scan 01 tree detection rates were clearly lower. The shorter scanning path resulted in the higher number of detected trees but the lower proportion of matching tree pairs (Figure 7). The rigid option for Scan 01 produced a point cloud below assumable standards as commission and omission errors rates surpassed the 30% threshold and the proportion of false positives almost reached 200 trees. The maximum allowed distance of 2 m for creating matching tree pairs was achieved similarly for both options in Scan 02. Most of the matches occurred under 50 cm distance between reference tree and detected tree, showing a proper alignment of HLS data with the reference coordinate system used for field work. For the case of Scan 01, the progress of the none-rigid option was similar as Scan 02 but it reached a lower asymptotic value (306 trees) compared to Scan 02 (394 and 412 pairs, respectively).
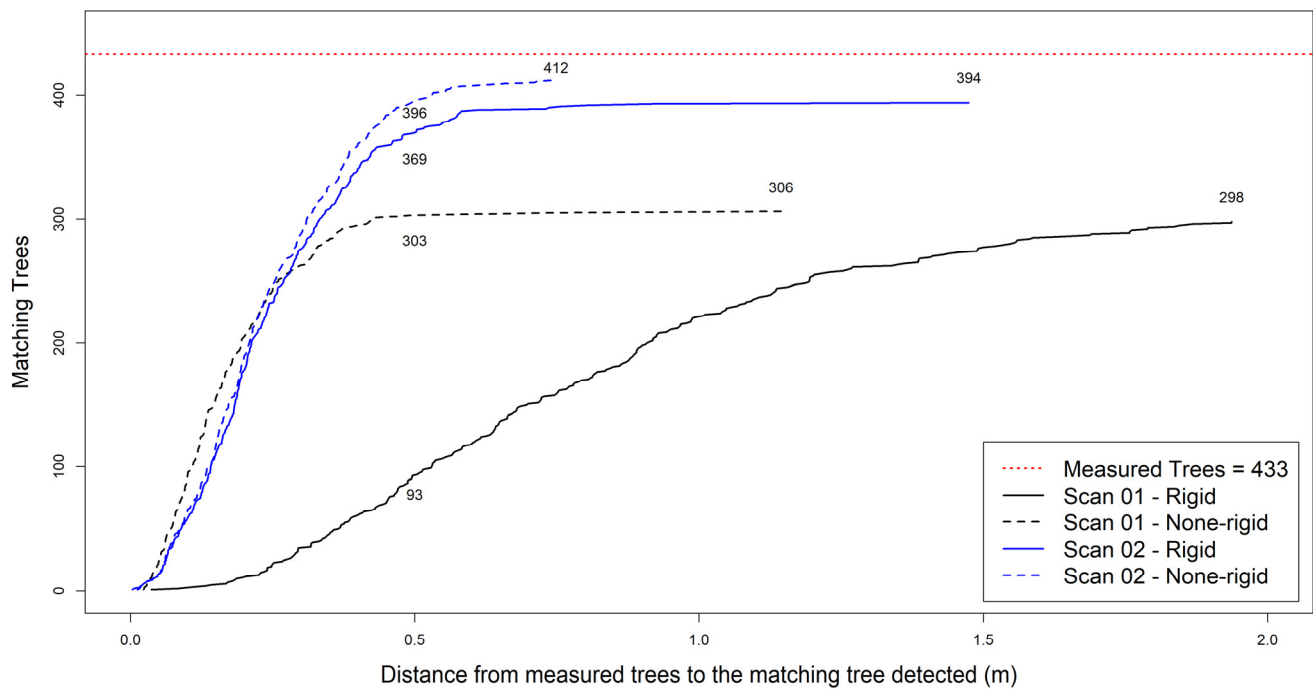
**Figure 6.** Diagram illustrating the number of matching tree pairs created on the *y*-axis and distance at which the matching is created on the *x*-axis. Distance between detected and reference trees was computed in the 2D space using detected locations from tree stems detected in FSCT and the measure locations during the field campaign. The maximum distance allowed for creating matching pairs was 2 m. Results are presented for two scans (Scan 01 and Scan 02) and two-point cloud transformation modes (rigid and none-rigid).

**Table 4.** Summary of tree detection results processed by FSCT for each of the four scans tested (Scan 01 and Scan 02 under the rigid and none-rigid transformation mode, respectively).

| Section | Scan 01 | | Scan 02 | |
|---|---|---|---|---|
| | **None-Rigid** | **Rigid** | **None-Rigid** | **Rigid** |
| Measured trees | 433 | 433 | 433 | 433 |
| Detected Tree | 509 | 316 | 407 | 426 |
| Number of matching pairs | 318 | 306 | 394 | 412 |
| False detected trees | 191 | 10 | 13 | 14 |
| Undetected trees | 115 | 127 | 39 | 21 |
| Commission errors (%) | 37.5% | 3.2% | 3.2% | 3.3% |
| Omission errors (%) | 26.6% | 29.3% | 9.0% | 4.8% |
| Overall accuracy (%) | 51% | 69% | 88% | 92% |

We used sections to break down the values for 1 ha forest (Figure 8). Tree detection rates were consistently above the 90% for Scan 02 under the none-rigid options, outperforming the rigid approach both in dense tree canopy conditions and also for sections with a few trees. Scan 02 achieved a detection rate of 95% for dense areas, regardless of mean DBH values or clustering of trees in the sections as informed by the CE index. As documented before, we found more variability and lower detection rates for Scan 01 although some section showed high values comparable to Scan 02. We present the omission and commission errors at section level as a map in the Appendix B including point cloud density.
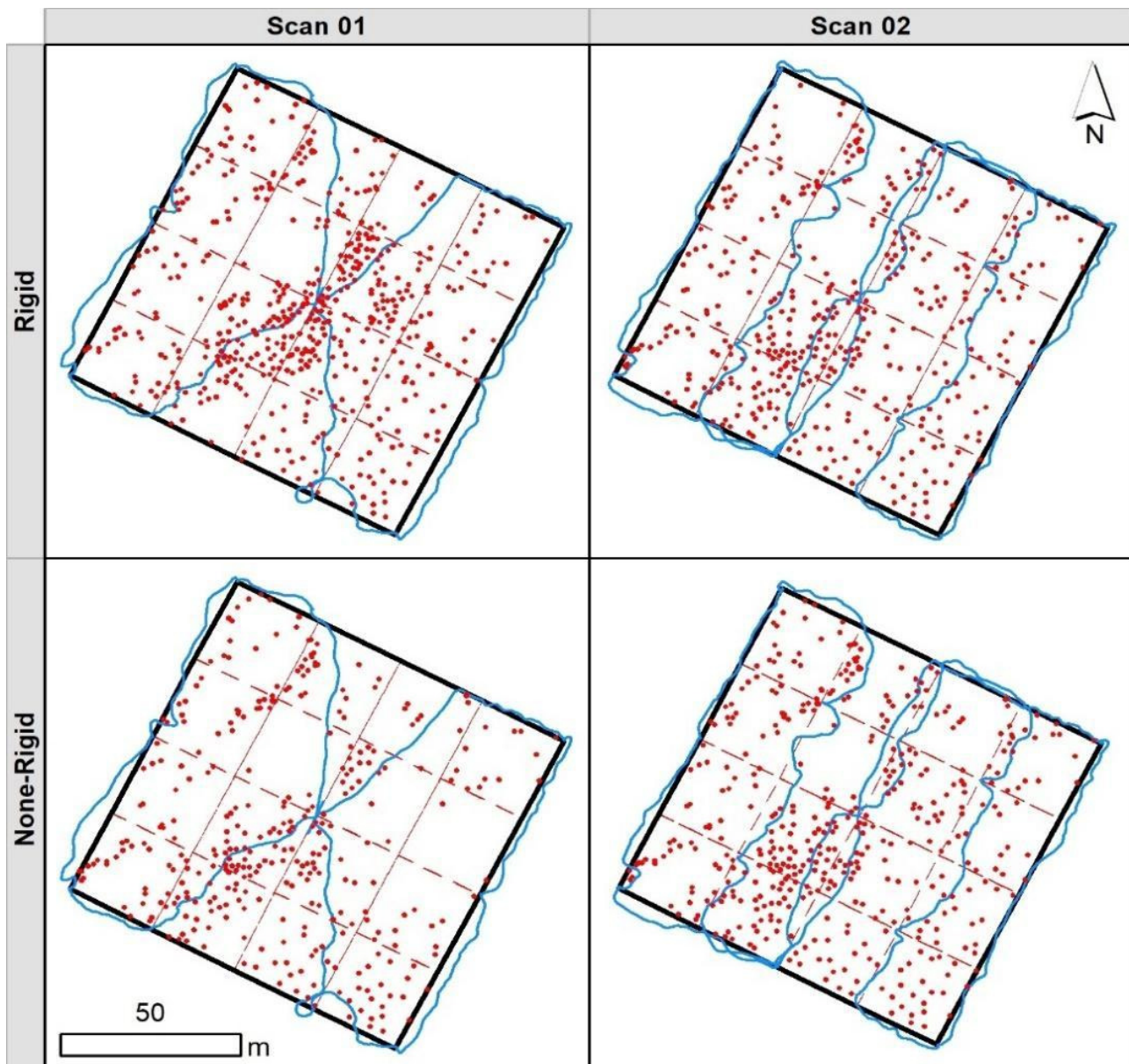
**Figure 7.** Spatial arrangement of tree matching pairs for Scan 01 and Scan 02 under the two transformation modes tested. For representation we used the coordinates of the detected tree for each pair. The scanning path is presented in blue colour for the four options tested, marteloscope are represented in solid black and sections' boundaries (16) are represented in dashed red colour.

### 3.4. Estimation of Diameter at Breast Height

RMSE values for DBH estimation are below 10% for Scan 02 (Table 5). The best performance for Scan 02 was observed when error decreased down to 6.5% for *Pinus pinaster* observations in the none-rigid mode. For Scan 01, we found the best performance for *Quercus pyrenaica* trees. In general, the none-rigid mode produced equivalent estimates for the two scanning paths tested: the $R^2$ values were consistently above 0.8 for cases considering tree density and species. The scatterplots showed the high impact of very few outliers in the computation of RMSE values (Figure 9). The 1:1 tendency remains consistent for all cases involving Scan 02 and for none-rigid options in Scan 01. The scatterplots confirmed the similar predictive capability of both transformation modes over the longer Scan 02 design.

| Subplot | Density | DBH (cm) | Height (m) | Scan 01 Rigid | | Scan 01 None-Rigid | | Scan 02 Rigid | | Scan 02 None-Rigid | |
|---|---|---|---|---|---|---|---|---|---|---|---|
| 1 | 22 | 31.37 | 19.64 | 19 | 86% | 16 | 73% | 12 | 55% | 22 | 100% |
| 2 | 33 | 28.76 | 17.87 | 19 | 58% | 21 | 64% | 30 | 91% | 31 | 94% |
| 3 | 12 | 32.60 | 19.08 | 3 | 25% | 9 | 75% | 11 | 92% | 12 | 100% |
| 4 | 15 | 43.54 | 22.09 | 6 | 40% | 11 | 73% | 15 | 100% | 15 | 100% |
| 5 | 30 | 27.99 | 18.51 | 19 | 63% | 25 | 83% | 27 | 90% | 29 | 97% |
| 6 | 15 | 20.32 | 13.83 | 9 | 60% | 6 | 40% | 12 | 80% | 11 | 73% |
| 7 | 36 | 27.68 | 18.76 | 31 | 86% | 16 | 44% | 30 | 83% | 33 | 92% |
| 8 | 16 | 46.93 | 22.06 | 11 | 69% | 2 | 13% | 16 | 100% | 15 | 94% |
| 9 | 21 | 33.07 | 18.45 | 11 | 52% | 17 | 81% | 19 | 90% | 19 | 90% |
| 10 | 53 | 17.99 | 13.49 | 43 | 81% | 40 | 75% | 49 | 92% | 52 | 98% |
| 11 | 33 | 28.50 | 18.11 | 31 | 94% | 25 | 76% | 32 | 97% | 33 | 100% |
| 12 | 22 | 40.62 | 21.47 | 20 | 91% | 11 | 50% | 21 | 95% | 21 | 95% |
| 13 | 30 | 28.91 | 20.38 | 9 | 30% | 28 | 93% | 27 | 90% | 27 | 90% |
| 14 | 49 | 20.93 | 16.27 | 24 | 49% | 36 | 73% | 48 | 98% | 47 | 96% |
| 15 | 22 | 43.73 | 20.85 | 21 | 95% | 20 | 91% | 22 | 100% | 22 | 100% |
| 16 | 24 | 35.88 | 21.62 | 22 | 92% | 23 | 96% | 23 | 96% | 23 | 96% |
| Total | 433 | 31.80 | 18.91 | 298 | 69% | 306 | 71% | 394 | 91% | 412 | 95% |

| | | | ≥ 75% | | | | ≥ 25% |
|---|---|---|---|---|---|---|---|
| | | | ≥ 50% | | | | ≥ 0% |

**Figure 8.** Assessment of tree detection accuracy using the 16 sections (subplots) conforming the 1 ha marteloscope. Control factors presented are mean diameter at breast height in the section (DBH), mean tree height and stem density. The number of trees detected (white background) and the percentage over the number of existing reference trees in the section (shaded background) are presented for the two scans (Scan 01 and Scan 02) and the two-point cloud transformation modes tested (rigid and none-rigid). Intervals of 25th percentiles were used for the legend to rank section values of tree density (one, two, three and four bars for each quarter), DBH (white, green, yellow and red from low to high density) and tree height (red down, yellow pointing down, yellow pointing up, and green up for lower to taller trees) over the array of 16 section values for the marteloscope.

**Table 5.** Summary statistics for the estimation of DBH using matching tree pairs using linear regression. Detected DBH estimates were used to estimate DBH measurements. Fitting statistics and number of observations (n) are presented for each species (*Alnus glutinosa* (Ag), *Pinus pinaster* (Pp) and *Quercus pyrenaica* (Qp)), scan transformation mode and for the tested scanning paths (Scan 01 and Scan 02).

| Scan | Transformation Mode | Species | n | $R^2$ | RMSE (cm) | RMSE (%) |
|---|---|---|---|---|---|---|
| Scan 01 | Rigid | Ag | 34 | 0.070 | 7.848 | 22.229 |
| | | Qp | 96 | 0.431 | 7.142 | 16.279 |
| | | Pp | 169 | 0.302 | 5.992 | 25.922 |
| | None-Rigid | Ag | 54 | 0.868 | 3.339 | 9.451 |
| | | Pp | 74 | 0.837 | 3.818 | 8.723 |
| | | Qp | 156 | 0.965 | 1.444 | 5.996 |
| Scan 02 | Rigid | Ag | 49 | 0.656 | 5.140 | 14.214 |
| | | Pp | 105 | 0.810 | 4.120 | 9.303 |
| | | Qp | 214 | 0.930 | 1.974 | 8.543 |
| | None-Rigid | Ag | 54 | 0.861 | 3.377 | 9.461 |
| | | Pp | 105 | 0.906 | 2.905 | 6.566 |
| | | Qp | 225 | 0.895 | 2.417 | 10.418 |
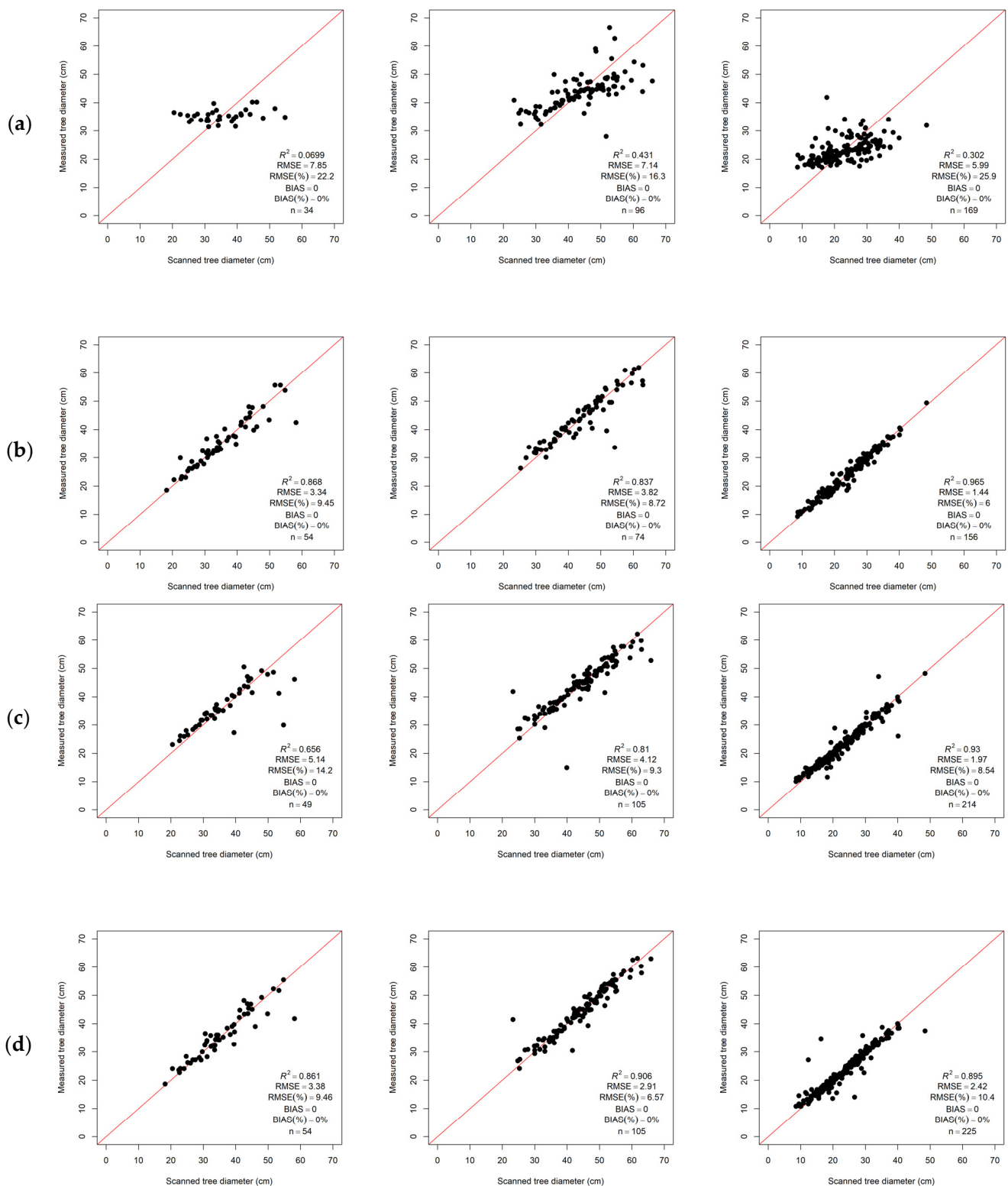
**Figure 9.** Predicted versus observed diameter at breast height using matching tree pairs. Results are presented for Scan 01 in Rigid and None-rigid modes ((**a**,**b**), respectively), and for Scan 02 ((**c**,**d**), respectively). First column is *Alnus glutinosa* (Ag), second column is *Pinus pinaster* (Pp) and third column represent observations of *Quercus pyrenaica* (Qp). Root mean squared errors are presented in cm, same scale as model estimates and measurements.

### 3.5. Estimation of Tree Height

The relations between predicted and measured tree height considerably differed from the previous results on DBH estimation (Table 6). The summary statistics showed relative RMSE values below 10% in some cases as for DBH but in general the tree height error rates were consistently higher. For Scan 02, the computed error rates followed similar patterns. We observed lower errors in Pp observations compared to broadleaf species: Ag in the range of 12% and above 20% for Qp observations for the two cases. Summary values presented in the table were compared with ALS-based measurements on height to confirm these two issues identified and to clarify whether tree height reference values or HLS data were the cause of the poor 1:1 relation observed in the scatterplots.

**Table 6.** Summary statistics for the estimation of tree height using matching tree pairs using linear regression. Detected tee heights were used to estimate field measurements. Fitting statistics and number of observations (n) are presented for each species, scan transformation mode and for the tested scanning paths (Scan 01 and Scan 02).

| Scan | Transformation Mode | Species | n | $R^2$ | RMSE (m) | RMSE (%) |
|---|---|---|---|---|---|---|
| Scan 01 | Rigid | Ag | 34 | 0.003 | 3.046 | 14.105 |
| | | Qp | 96 | 0.043 | 2.227 | 10.092 |
| | | Pp | 169 | 0.159 | 3.656 | 20.965 |
| | None-Rigid | Ag | 54 | 0.006 | 3.822 | 17.513 |
| | | Pp | 74 | 0.034 | 2.073 | 9.390 |
| | | Qp | 156 | 0.196 | 3.703 | 21.097 |
| Scan 02 | Rigid | Ag | 49 | 0.404 | 2.626 | 12.010 |
| | | Pp | 105 | 0.217 | 1.956 | 8.846 |
| | | Qp | 214 | 0.169 | 3.715 | 21.632 |
| | None-Rigid | Ag | 54 | 0.325 | 3.192 | 14.746 |
| | | Pp | 105 | 0.212 | 1.961 | 8.869 |
| | | Qp | 225 | 0.142 | 3.732 | 21.610 |

### 3.6. Airborne Laser Data to Assess HLS Tree Heights

Height statistics from ALS show agreement to HLS-based estimates (Figure 10), confirming the likely occurrence of measurement errors in the field. We used crown width measurements in the field and detected tree positions to calculate the ground projection of the canopy for each reference tree in a matching pair and isolate ALS echoes. Beyond systematic differences between measurements and estimates, we assess the linearity of specific height distributions for the three species. The results for Qp showed how field measurements underestimated tree heights as we confirmed the agreement between ALS and HLS data—1:1 relation is strong in the figures. The presence of observations beyond the 1:1 tendency line was caused by the leaf-off conditions of the ALS data. The same was observed for Ag but not for evergreen Pp species as expected. Matching tree pairs identified as Pp for the four alternatives tested showed similar trends for tree heights and the agreement between HLS and ALS data was strong, showing the agreement between two sources of scanning. Focusing on Scan 02, the relations were very similar and with no presence of outliers, suitable conditions to verify the correspondence of ALS to HLS information. The comparison between ALS and HLS showed slightly lower values for HLS height estimates as expected (Figure 10). We discuss later the role of phenology in our results, the effect of acquisition times for both ALS and field data, and the challenging operation of verifying height estimates from remote sensing products using field data collected in difficult conditions.
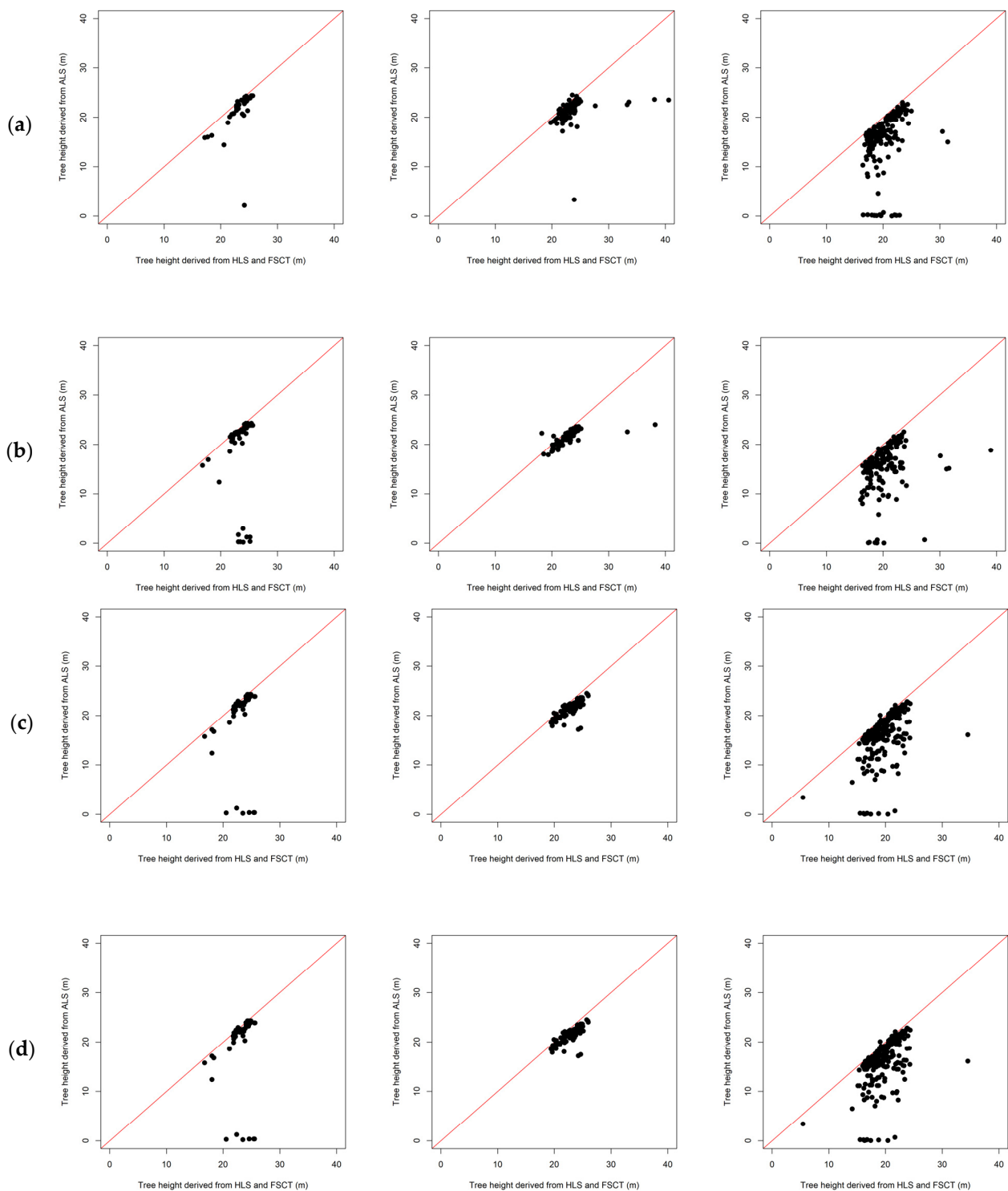
**Figure 10.** Relationship between scanned height using handheld laser scanning (HLS) and the Forest Complexity Tool and height estimates from airborne laser data (ALS). Results are presented for Scan 01 in rigid and none-rigid modes ((**a**,**b**), respectively), and for Scan 02 ((**c**,**d**), respectively). First column is *Alnus glutinosa* (Ag), second column is *Pinus pinaster* (Pp) and third column represent observations of *Quercus pyrenaica* (Qp).

## 4. Discussion

The combined performance of HLS data and FSCT was good for the study site regarding the positioning of detected trees. The tree detection rates of 88% and 92% for Scan 02 are satisfactory considering the challenging conditions we faced in this experiment. Values above 95% in tree detection have been reported in HLS and TLS studies but in different forest ecosystems [2,8,9,13,49]. The longer scanning path resulting in a denser point cloud provide better results as expected—only one and two sections of the 16 composing the experiment had tree detection rates below 90% for Scan 02 in the none-rigid and rigid transformation modes tested. Still, the performance of Scan 01 in tree detection and estimation of tree structural attributes was close in some sections, showing the value of the none-rigid transformation method. In terms of positioning accuracy, most detected trees were within 0.5 m of the location measured with a total station in the field, proving the agreement in geolocation of ground truth data to laser-based detection using FSCT.

The challenging conditions of the plot are representative of Mediterranean mixed forests and they bring complexity to the operationalization of the scan, the collection of field data and the calibration of scanned data. Conditions for this experiment were more complex than in reference papers in the field [17,19,31,45,50,51]. The studies from [29] and [16] used one plot to determine the goodness of HLS-based tree mapping. Several factors cannot be assessed in such a limited experimental design such as scanning path, and degrees of freedom needed to model measured and estimated information are few. We expanded the knowledge of HLS-based mapping in Mediterranean forests using a reference dataset of more than 400 trees over 1 ha, conditions for which scanning path and transformation mode must be carefully designed. We showed the variability in pulse density and the influence it has on the presence of commission and omission errors. Under Scan 02, the distribution of omission and commission errors was similar regardless on the transformation mode. The Figure A1 shows how sections closer or transited during the scanning operation in Scan 02 had lower errors compared to Scan 01.

In this study, our aim is to inform practitioners on operational factors such as computing time, scanning time in the field and scale of the database we handled. This is important and somehow lacking in scientific papers on the HLS-based approach except in a few relevant studies (i.e., [11]). It took 1 h and 10 min to both survey in the field under Scan 02 and create the point cloud in the lab. The acquisition time of 22 min is under the upper bound for continuous scanning time suggested by the manufacturer (30 min). We used a total station to geolocate ground control points rather than using a less time-consuming GNSS solution. We used the former to ensure more accuracy in this experiment and also to better register the ALS data available for height validation purposes. In terms of DBH estimation, the presence of a few outliers worsened the overall good alignment of detected information to DBH measurements despite the high variability in allometries for *Quercus pyrenaica* and *Alnus glutinosa* compared to the more consistent stem profiles of *Pinus pinaster* in the plot. High variability in tree allometries is common in mixed, irregular forests where DBH and tree height relationship can change from competition or forest management, among other factors [23,34,52]. The results for Scan 02 were similar and the error values for our study are in accordance to previous studies conducted in different forest ecosystems [13,16,41]. In this regard, recent studies suggest enhanced procedures for DBH calibration and estimation of cross-sectional (cross-section area estimation, [53]). The estimation of DBH using HLS data and FSCT was good and substantially less complex to interpret and validate compared to tree height.

Measuring tree height for calibrating and validating remote sensing data is complex [6,18,37]. The assumption that laser scanning data tends to underestimate tree height is supported by previous research evaluating the use of TLS (e.g., [54]), ALS surveys [1,48] and HLS data (Table A1). Tree heights measurements are highly susceptible to errors [6]. Challenging conditions during field observation of tree height, e.g., uneven-aged forests, closed canopies, high stocking densities, etc., can trigger larger deviations between ground truth and observed ground truth [18,24]. These factors may have exacer-

bated errors in tree height measurement in our training area while operating the vertex, which is a standard solution in the field to get height measurements.

Conditions in the area regarding species composition, crown intersections and multi-layered conditions are likely to introduce discrepancies between ground measurements and true height values. Moreover, the field campaign used for height measurements took place in leaf-on conditions, adding more complexity to the interpretation of the patterns presented for tree height. Fortunately, the use of leaf-off ALS data for validation was enough to allow us to bring light to this issue and to better explain differences between species. It also helped to validate the reliability of the HLS-based approach for tree height mapping and emphasize the need to carefully evaluate the source of data set as reference—ALS, HLS or field data in our case. The similarity of point clouds for HLS and ALS data for evergreen pine trees showed both scanners were able to detect tree attributes similarly. Cross-comparisons between the three height estimates, field data, ALS-based height data and the results from HLS present a high agreement (<1 m) and lower rRMSE values for evergreen pines. It has been established that ALS systems tend to underestimate tree height [55], which is consequence of the operation of the scanner and the inadequate representation of canopy apices due to low point density [56,57], seasonal conditions and ALS-based DTM to normalize the height. These reasons could probably explain that HLS tended to slightly overestimate ALS height in our case. Despite the considerably high density of ALS data in our case (>10 points $m^{-1}$), the height of some trees was not captured, as trees were in leaf-off conditions during the ALS survey. However, oak trees were in leaf-on conditions during field work and errors from occlusion should be expected when comparing heights from the HLS data to the field measurement. The pattern is especially clear here for Qp but also for the other two species. Qp species have high resprouting capabilities and could present several numbers of sprouts or shoots for the same stump (Figure 2). The relationships presented in Figure 10 suggest tree height measurements suffered mainly from under-estimation errors, which are more evident in deciduous trees, as field work was carried out when canopy closure represented a problem for the measuring team.

The study from [40] performed an enhanced segmentation of tree canopies to address the tree height estimation problem, reducing error rates below 1.5 m for the whole experiment compared to height measurements measured with the same instrument we used—assumed as reference. The approach is promising and followed in recent studies [58] and authors reported better results than us considering all species, so their method can improve our results on tree height. We want to be transparent on tree height results as we find that tree height is not always reported in HLS- or TLS-based studies which tend to focus more on tree detection and estimation of DBH [6,59]. Considering the similarity between ALS and HLS data and the comparison between laser data and field measurements for the other two species, we suggest that tree height measurements in the field should be carefully evaluated when it comes to reference values and to decide whether field data should be considered as truth values. These findings inform ongoing debates in the forest remote sensing community about what to consider as reference data [18,19,37]. We confirmed this issue by using ALS and HLS together and acknowledging differences in phenology for the species.

Finally, we want to emphasize the importance of ALS data to support terrestrial laser data, e.g., TLS and HLS, as well as field measurements. Nowadays, ALS surveys are available in many countries both from private and public sources. This is the case in Spain where the multi-temporal LiDAR PNOA project is growing more useful for forestry application with ALS point cloud densities set to increase from 1–2 points $m^{-1}$ up to 5 points $m^{-1}$ for acquisition flights scheduled between 2022 and 2025 [48,60]. The nominal point density for the marteloscope was 2 points but the real density was above 10 points, which is enough to conduct tree detection from the ALS. The refinement of ALS programs towards high-resolution data will increase the possibilities to support forest planning (e.g., [61])

and to better optimize the usability of point clouds by combining laser echoes from TLS, HLS and ALS systems.

## 5. Conclusions

This study expands the state of the art of HLS-based mapping in Mediterranean forests. The study provides insights and recommendations on the point cloud processing routines and uses ALS data to further test the performance of tree height detection, the most challenging variable estimated in the study and in tree level mapping in general. Using optimal and time-efficient scanning tracks, we showed how HLS and FSCT can render tree detection rates above 90% at a high-precision for tree positioning and DBH estimation. Species composition and phenology affected the accuracy of HLS-based mapping depending on the structural variable assessed. The addressing of field reference errors for height was an issue but adding ALS data to the validation helped to reduce uncertainty in the evaluation of the HLS approach as a flexible, functional and time-efficient technology to support tree mapping surveys—with a high potential to support permanent sampling in the near future for programs such as national forest inventories.

**Author Contributions:** Conceptualization, F.T.-S.; methodology, F.T.-S.; formal analysis, F.T.-S. and A.P.; resources, F.B. and C.O.; writing—original draft preparation, F.T.-S.; writing—review and editing, F.T.-S., A.P., J.G.-H., C.O., T.d.C. and F.B.; supervision, F.B., A.P. and J.G.-H.; project administration, F.B.; funding acquisition, F.B. All authors have read and agreed to the published version of the manuscript.

**Data Availability Statement:** As previously stated, this dataset is available for public use here at Zenodo. The Digital Object Identifier (DOI) of this dataset is https://doi.org/10.5281/zenodo.6382661. As a backup, the same dataset is also stored at the University of Valladolid. If the above link no longer gives you access to the dataset, please contact Frederico Simões via his permanent email address at fredericotupinamba@hotmail.com, and he will send you the dataset directly.

**Conflicts of Interest:** The authors declare no conflict of interest.

## Appendix A

**Table A1.** Summary results of HLS-based forest inventory studies.

| Region | Sensor | Formations | Number of Plots | Tree Detection, Producer's Accuracy (Commission, Omission) | Variable | Bias (in Unit for Each Variable) | Accuracy of Extended Attributes (RMSE, rRMSE) | Ref |
|---|---|---|---|---|---|---|---|---|
| Belgium | ZEB1 | *B: broadleaveC: Coniferous M: mixed* | 10 (15 m diameter) | 90% ± 12% −21% | DBH | 0.08 | 1.11 (4.1%) | [2] |
| Germany | Riegl VMX-250 | *Mixed forest* | 2 (radius 12.62 m) | Plot 3 87.5% | DBH | | 3.7 | [13] |
| | | | | Plot 2 (100%, 49) | CPA | underest. | 2.2 m² | |
| | | | | | V | underest. | 0.4 m³ and 0.6 m³ | |

**Table A1.** *Cont.*

| Region | Sensor | Formations | Number of Plots | Tree Detection, Producer's Accuracy (Commission, Omission) | Variable | Bias (in Unit for Each Variable) | Accuracy of Extended Attributes (RMSE, rRMSE) | Ref |
|---|---|---|---|---|---|---|---|---|
| Spain | ZEB-REVO | *P. pinea and Platanus hispanica* | 1 (1 ha), 277 trees | - | DBH | −0.1 | 1.1 | [62] |
| | | | | | H | 0.94 | 1.34 | |
| | | *Pinus sylvestris* | 1 (0.5 ha) | - | DBH | −0.1 | 0.9 | |
| | | | | | H | −9 | 9.44 | |
| Italy | ZEB1 | *Mediterranean multi-layered forest* | 1 (r = 13 m) | 100% | DBH | −0.38 | 1.28 | [29] |
| | | | | | H | −4.61 | 2.15 | |
| | | | | | CBH | 1.67 | 1.91 | |
| | | | | | CPA | 0.25 | 0.59 | |
| Norway | ZEB1 | *Picea abies P. sylvestris, Betula pubescens* | 7 (500 m², 335) | 74% (4.8%, 26%) | DBH | 0.3 | 3.1 (14.3%) | [31] |
| China | ZEB-REVORT | *Styphnolobium japonicum* | 1 rectangular (300 m², 30 trees) | 93.3% (6.1%) | DBH | −1.26 | 1.58 (11.8%) | [14] |
| Italy | *ZEB1* | *Pure culture stand; Castanea sativa* | 3 circular plots (r = 30 m, 98 trees) | 93% (6% omission) | DBH | −0.22 | 2.5 cm | [16] |
| | | | | | H (<10–20 m) | 0.16 | 0.67 (6.52%) | |
| | | | | | CBH | −0.14 | 0.30 (11.12%) | |
| | | | | | H | 4.026 | 4.026 | |
| Austria | ZEB-HORIZON | *broadleaved, coniferous, mixed)* | 20 circular(r = 20 m) | 96% (0.62, 1.62%) | DBH | 0.21 | 2.32 (12.01%) | [11] |
| Finland | ZEB-HORIZON | *Boreal,coniferous-dominated,mixed stands* | sparse (32 × 32 m, 42 trees) | Plot1 | DBH | −0.39 and −1.44 | 0.9 (3.5%) and 1.3 (4.2%) | [17] |
| | | | | 87.5% | H | −0.16 and −1.1 | 0.4 (1.6%) and 1.4 (5.7%) | |
| | | | Obstructed stand (32 × 3 2 m, 43 trees) | Plot 2 100% | V | 37 dm³ and 5 dm³ | 71 dm³ (11.5%) and 81 dm³ (8.9%) | |
| U.S. | ZEB-HORIZON | *Pinus ponderosa* | 12 circular plots (0.04 ha, 209 trees) | 94.7% (8.5%, 1.8%) | DBH | overestimation | 4.8 (25.9%) | [41] |
| | | | | | H | overestimation | 1.3 (14.2%) | |
| Italy | Kaarta Stencil 2.1 | *Pinus nigra* | 0.5 ha 50 trees | - | DBH | 0.01 | 10.8% | [21] |
| | | | | | CBH | −1.48 | 13.9% | |
| | | | | | H | −1.2 | 14.7% | |
| Italy | ZEB-HORIZON | Mixed forest | 20 plots (r = 15.20, 25 m) | - | DBH | 2.401 | 3.52 | [9] |

**Appendix B**
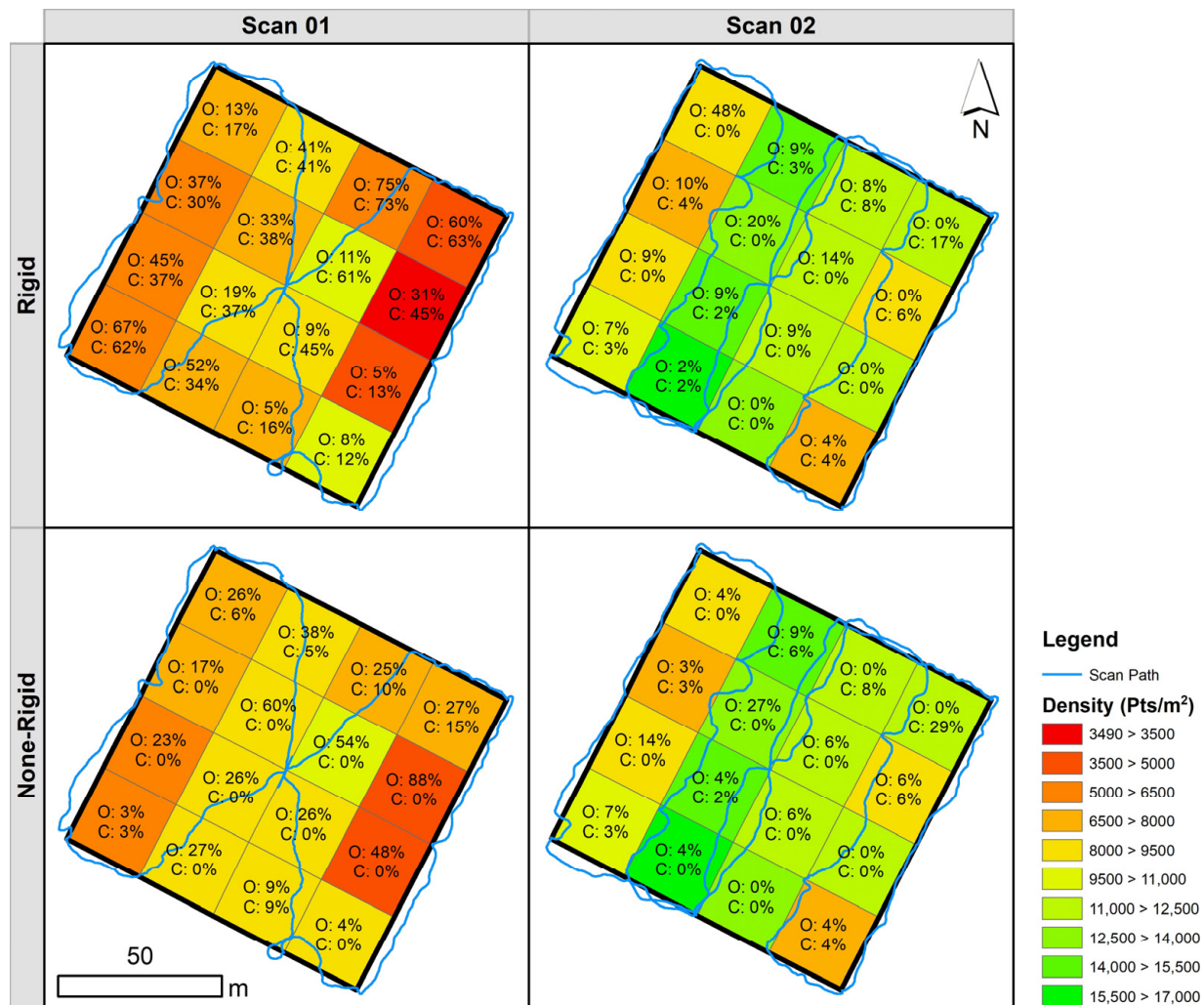


**Figure A1.** Representation of scanning density (coloured background) and commission and omission errors in the study. The latter two are shown as percentages for each section of the forests (O: omission: C: commission).

## References

1.  Maltamo, M.; Næsset, E.; Vauhkonen, J. (Eds.) *Forestry Applications of Airborne Laser Scanning: Concepts and Case Studies*; Managing Forest Ecosystems; Springer: Dordrecht, The Netherlands, 2014; Volume 27, ISBN 978-94-017-8662-1.
2.  Bauwens, S.; Bartholomeus, H.; Calders, K.; Lejeune, P. Forest Inventory with Terrestrial LiDAR: A Comparison of Static and Hand-Held Mobile Laser Scanning. *Forests* **2016**, *7*, 127. [CrossRef]
3.  Maas, H.-G.; Bienert, A.; Scheller, S.; Keane, E. Automatic Forest Inventory Parameter Determination from Terrestrial Laser Scanner Data. *Int. J. Remote Sens.* **2008**, *29*, 1579–1593. [CrossRef]
4.  Liang, X.; Litkey, P.; Hyyppa, J.; Kaartinen, H.; Vastaranta, M.; Holopainen, M. Automatic Stem Mapping Using Single-Scan Terrestrial Laser Scanning. *IEEE Trans. Geosci. Remote Sens.* **2012**, *50*, 661–670. [CrossRef]
5.  Almeida, A.; Gonçalves, F.; Silva, G.; Mendonça, A.; Gonzaga, M.; Silva, J.; Souza, R.; Leite, I.; Neves, K.; Boeno, M.; et al. Individual Tree Detection and Qualitative Inventory of a Eucalyptus Sp. Stand Using UAV Photogrammetry Data. *Remote Sens.* **2021**, *13*, 3655. [CrossRef]
6.  Persson, H.J.; Olofsson, K.; Holmgren, J. Two-Phase Forest Inventory Using Very-High-Resolution Laser Scanning. *Remote Sens. Environ.* **2022**, *271*, 112909. [CrossRef]
7.  Calders, K. Terrestrial Laser Scanning for Forest Monitoring. PhD Thesis, Wageningen University, Wageningen, NL, USA, 2015. [CrossRef]

8.  Liang, X.; Hyyppä, J.; Kaartinen, H.; Lehtomäki, M.; Pyörälä, J.; Pfeifer, N.; Holopainen, M.; Brolly, G.; Francesco, P.; Hackenberg, J.; et al. International Benchmarking of Terrestrial Laser Scanning Approaches for Forest Inventories. *ISPRS J. Photogramm. Remote Sens.* **2018**, *144*, 137–179. [CrossRef]

9.  Sofia, S.; Maetzke, F.G.; Crescimanno, M.; Coticchio, A.; La Mela Veca, D.S.; Galati, A. The Efficiency of LiDAR HMLS Scanning in Monitoring Forest Structure Parameters: Implications for Sustainable Forest Management. *EuroMed J. Bus.* **2022**, *17*, 350–373. [CrossRef]

10. Gollob, C.; Ritter, T.; Nothdurft, A. Forest Inventory with Long Range and High-Speed Personal Laser Scanning (PLS) and Simultaneous Localization and Mapping (SLAM) Technology. *Remote Sens.* **2020**, *12*, 1509. [CrossRef]

11. Gollob, C.; Ritter, T.; Nothdurft, A. Comparison of 3D Point Clouds Obtained by Terrestrial Laser Scanning and Personal Laser Scanning on Forest Inventory Sample Plots. *Data* **2020**, *5*, 103. [CrossRef]

12. 12. Liang, X.; Kukko, A.; Balenovic, I.; Saarinen, N.; Junttila, S.; Kankare, V.; Holopainen, M.; Mokros, M.; Surovy, P.; Kaartinen, H.; et al. Close-Range Remote Sensing of Forests: The State of the Art, Challenges, and Opportunities for Systems and Data Acquisitions. *IEEE Trans. Geosci. Remote Sens.* **2022**, *10*, 32–71. [CrossRef]

13. Bienert, A.; Georgi, L.; Kunz, M.; Maas, H.-G.; von Oheimb, G. Comparison and Combination of Mobile and Terrestrial Laser Scanning for Natural Forest Inventories. *Forests* **2018**, *9*, 395. [CrossRef]

14. Chen, S.; Liu, H.; Feng, Z.; Shen, C.; Chen, P. Applicability of Personal Laser Scanning in Forestry Inventory. *PLoS ONE* **2019**, *14*, e0211392. [CrossRef] [PubMed]

15. Balenović, I.; Liang, X.; Jurjević, L.; Hyyppä, J.; Seletković, A.; Kukko, A. Hand-Held Personal Laser Scanning: Current Status and Perspectives for Forest Inventory Application. *Croat. J. For. Eng.* **2021**, *42*, 165–183. [CrossRef]

16. Del Perugia, B.; Giannetti, F.; Chirici, G.; Travaglini, D. Influence of Scan Density on the Estimation of Single-Tree Attributes by Hand-Held Mobile Laser Scanning. *Forests* **2019**, *10*, 277. [CrossRef]

17. Hyyppä, E.; Yu, X.; Kaartinen, H.; Hakala, T.; Kukko, A.; Vastaranta, M.; Hyyppä, J. Comparison of Backpack, Handheld, Under-Canopy UAV, and Above-Canopy UAV Laser Scanning for Field Reference Data Collection in Boreal Forests. *Remote Sens.* **2020**, *12*, 3327. [CrossRef]

18. Fan, Y.; Feng, Z.; Mannan, A.; Khan, T.; Shen, C.; Saeed, S. Estimating Tree Position, Diameter at Breast Height, and Tree Height in Real-Time Using a Mobile Phone with RGB-D SLAM. *Remote Sens.* **2018**, *10*, 1845. [CrossRef]

19. Wang, Y.; Lehtomäki, M.; Liang, X.; Pyörälä, J.; Kukko, A.; Jaakkola, A.; Liu, J.; Feng, Z.; Chen, R.; Hyyppä, J. Is Field-Measured Tree Height as Reliable as Believed—A Comparison Study of Tree Height Estimates from Field Measurement, Airborne Laser Scanning and Terrestrial Laser Scanning in a Boreal Forest. *ISPRS J. Photogramm. Remote Sens.* **2019**, *147*, 132–145. [CrossRef]

20. Davison, S.; Donoghue, D.N.M.; Galiatsatos, N. The Effect of Leaf-on and Leaf-off Forest Canopy Conditions on LiDAR Derived Estimations of Forest Structural Diversity. *Int. J. Appl. Earth Obs. Geoinf.* **2020**, *92*, 102160. [CrossRef]

21. Chiappini, S.; Pierdicca, R.; Malandra, F.; Tonelli, E.; Malinverni, E.S.; Urbinati, C.; Vitali, A. Comparing Mobile Laser Scanner and Manual Measurements for Dendrometric Variables Estimation in a Black Pine (Pinus Nigra Arn.) Plantation. *Comput. Electron. Agric.* **2022**, *198*, 107069. [CrossRef]

22. Pretzsch, H. *Forest Dynamics, Growth and Yield: From Measurement to Model*; Springer: Berlin/Heidelberg, Germany, 2009; ISBN 978-3-540-88306-7.

23. Bravo-Oviedo, A.; Pretzsch, H.; Ammer, C.; Andenmatten, E.; Barbati, A.; Barreiro, S.; Brang, P.; Bravo, F.; Coll, L.; Corona, P.; et al. European Mixed Forests: Definition and Research Perspectives. *For. Syst.* **2014**, *23*, 518. [CrossRef]

24. Bravo, F.; Fabrika, M.; Ammer, C.; Barreiro, S.; Bielak, K.; Coll, L.; Fonseca, T.; Kangur, A.; Löf, M.; Merganičová, K.; et al. Modelling Approaches for Mixed Forests Dynamics Prognosis. Research Gaps and Opportunities. *For. Syst.* **2019**, *28*, eR002. [CrossRef]

25. López-Marcos, D.; Turrión, M.-B.; Bravo, F.; Martínez-Ruiz, C. Understory Response to Overstory and Soil Gradients in Mixed versus Monospecific Mediterranean Pine Forests. *Eur. J. For. Res.* **2019**, *138*, 939–955. [CrossRef]

26. Oveland, I.; Hauglin, M.; Gobakken, T.; Næsset, E.; Maalen-Johansen, I. Automatic Estimation of Tree Position and Stem Diameter Using a Moving Terrestrial Laser Scanner. *Remote Sens.* **2017**, *9*, 350. [CrossRef]

27. Sibona, E.; Vitali, A.; Meloni, F.; Caffo, L.; Dotta, A.; Lingua, E.; Motta, R.; Garbarino, M. Direct Measurement of Tree Height Provides Different Results on the Assessment of LiDAR Accuracy. *Forests* **2016**, *8*, 7. [CrossRef]

28. Chudá, J.; Kadlečík, R.; Mokroš, M.; Mikita, T.; Tuček, J.; Chudý, F. Slam and ins based positional accuracy assessment of natural and artificial objects under the forest canopy. *Int. Arch. Photogramm. Remote Sens. Spat. Inf. Sci.* **2022**, *43*, 197–205. [CrossRef]

29. Giannetti, F.; Puletti, N.; Quatrini, V.; Travaglini, D.; Bottalico, F.; Corona, P.; Chirici, G. Integrating Terrestrial and Airborne Laser Scanning for the Assessment of Single-Tree Attributes in Mediterranean Forest Stands. *Eur. J. Remote Sens.* **2018**, *51*, 795–807. [CrossRef]

30. Fan, W.; Liu, H.; Xu, Y.; Lin, W. Comparison of Estimation Algorithms for Individual Tree Diameter at Breast Height Based on Hand-Held Mobile Laser Scanning. *Scand. J. For. Res.* **2021**, *36*, 460–473. [CrossRef]

31. Oveland, I.; Hauglin, M.; Giannetti, F.; Schipper Kjørsvik, N.; Gobakken, T. Comparing Three Different Ground Based Laser Scanning Methods for Tree Stem Detection. *Remote Sens.* **2018**, *10*, 538. [CrossRef]

32. Krisanski, S.; Taskhiri, M.S.; Gonzalez Aracil, S.; Herries, D.; Muneri, A.; Gurung, M.B.; Montgomery, J.; Turner, P. Forest Structural Complexity Tool—An Open Source, Fully-Automated Tool for Measuring Forest Point Clouds. *Remote Sens.* **2021**, *13*, 4677. [CrossRef]

33. Schuck, A.; Kraus, D.; Krumm, F.; Held, A.; Schmitt, H. *Integrate+ Marteloscopes—Calibrating Silvicultural Decision Making*; Integrate+ Technical Paper; European Forest Institute: Barcelona, Spain, 2015; p. 12.

34. Pretzsch, H.; Zenner, E.K. Toward Managing Mixed-Species Stands: From Parametrization to Prescription. *For. Ecosyst.* **2017**, *4*, 19. [CrossRef]

35. MITECO 4rd Spanish National Forest Inventory in Extremadura.: Ministerio Para La Transición Ecológica y El Reto Demográfico 2020. Available online: https://www.miteco.gob.es/es/biodiversidad/temas/inventarios-nacionales/inventario-forestal-nacional/cuarto_inventario.aspx (accessed on 10 December 2022).

36. Erdody, T.L.; Moskal, L.M. Fusion of LiDAR and Imagery for Estimating Forest Canopy Fuels. *Remote Sens. Environ.* **2010**, *114*, 725–737. [CrossRef]

37. Andersen, H.-E.; Reutebuch, S.E.; McGaughey, R.J. A Rigorous Assessment of Tree Height Measurements Obtained Using Airborne Lidar and Conventional Field Methods. *Can. J. Remote Sens.* **2006**, *32*, 355–366. [CrossRef]

38. Roussel, J.-R.; Auty, D.; Coops, N.C.; Tompalski, P.; Goodbody, T.R.H.; Meador, A.S.; Bourdon, J.-F.; de Boissieu, F.; Achim, A. LidR: An R Package for Analysis of Airborne Laser Scanning (ALS) Data. *Remote Sens. Environ.* **2020**, *251*, 112061. [CrossRef]

39. R Core Team. *R: A Language and Environment for Statistical Computing*; R Core Team: Vienna, Austria, 2022.

40. Tockner, A.; Gollob, C.; Kraßnitzer, R.; Ritter, T.; Nothdurft, A. Automatic Tree Crown Segmentation Using Dense Forest Point Clouds from Personal Laser Scanning (PLS). *Int. J. Appl. Earth Obs. Geoinf.* **2022**, *114*, 103025. [CrossRef]

41. Donager, J.J.; Sánchez Meador, A.J.; Blackburn, R.C. Adjudicating Perspectives on Forest Structure: How Do Airborne, Terrestrial, and Mobile Lidar-Derived Estimates Compare? *Remote Sens.* **2021**, *13*, 2297. [CrossRef]

42. Kükenbrink, D.; Marty, M.; Bösch, R.; Ginzler, C. Benchmarking Laser Scanning and Terrestrial Photogrammetry to Extract Forest Inventory Parameters in a Complex Temperate Forest. *Int. J. Appl. Earth Obs. Geoinf.* **2022**, *113*, 102999. [CrossRef]

43. Krisanski, S.; Taskhiri, M.S.; Gonzalez Aracil, S.; Herries, D.; Turner, P. Sensor Agnostic Semantic Segmentation of Structurally Diverse and Complex Forest Point Clouds Using Deep Learning. *Remote Sens.* **2021**, *13*, 1413. [CrossRef]

44. Ester, M.; Kriegel, H.-P.; Xu, X. A Density-Based Algorithm for Discovering Clusters in Large Spatial Databases with Noise. *kdd* **1996**, *96*, 226–231.

45. Hyyppä, E.; Kukko, A.; Kaijaluoto, R.; White, J.C.; Wulder, M.A.; Pyörälä, J.; Liang, X.; Yu, X.; Wang, Y.; Kaartinen, H.; et al. Accurate Derivation of Stem Curve and Volume Using Backpack Mobile Laser Scanning. *ISPRS J. Photogramm. Remote Sens.* **2020**, *161*, 246–262. [CrossRef]

46. Guerra-Hernández, J.; Botequim, B.; Bujan, S.; Jurado-Varela, A.; Molina-Valero, J.A.; Martínez-Calvo, A.; Pérez-Cruzado, C. Interpreting the Uncertainty of Model-Based and Design-Based Estimation in Downscaling Estimates from NFI Data: A Case-Study in Extremadura (Spain). *GIScience Remote Sens.* **2022**, *59*, 686–704. [CrossRef]

47. rapidlasso GmbH. *"LAStools—Efficient LiDAR Processing Software"*, version 141017, commercial; rapidlasso GmbH: Gilching, Germany. Available online: http://rapidlasso.com/LAStools (accessed on 18 January 2023).

48. Pascual, A. Using Tree Detection Based on Airborne Laser Scanning to Improve Forest Inventory Considering Edge Effects and the Co-Registration Factor. *Remote Sens.* **2019**, *11*, 2675. [CrossRef]

49. Ryding, J.; Williams, E.; Smith, M.J.; Eichhorn, M.P. Assessing Handheld Mobile Laser Scanners for Forest Surveys. *Remote Sens.* **2015**, *7*, 1095–1111. [CrossRef]

50. Holopainen, M.; Kankare, V.; Vastaranta, M.; Liang, X.; Lin, Y.; Vaaja, M.; Yu, X.; Hyyppä, J.; Hyyppä, H.; Kaartinen, H.; et al. Tree Mapping Using Airborne, Terrestrial and Mobile Laser Scanning—A Case Study in a Heterogeneous Urban Forest. *Urban For. Urban Green.* **2013**, *12*, 546–553. [CrossRef]

51. Luoma, V.; Saarinen, N.; Wulder, M.; White, J.; Vastaranta, M.; Holopainen, M.; Hyyppä, J. Assessing Precision in Conventional Field Measurements of Individual Tree Attributes. *Forests* **2017**, *8*, 38. [CrossRef]

52. Tong, Q.J.; Zhang, S.Y. Stem Form Variations in the Natural Stands of Major Commercial Softwoods in Eastern Canada. *For. Ecol. Manag.* **2008**, *256*, 1303–1310. [CrossRef]

53. Witzmann, S.; Matitz, L.; Gollob, C.; Ritter, T.; Kraßnitzer, R.; Tockner, A.; Stampfer, K.; Nothdurft, A. Accuracy and Precision of Stem Cross-Section Modeling in 3D Point Clouds from TLS and Caliper Measurements for Basal Area Estimation. *Remote Sens.* **2022**, *14*, 1923. [CrossRef]

54. Liang, X.; Kankare, V.; Hyyppä, J.; Wang, Y.; Kukko, A.; Haggrén, H.; Yu, X.; Kaartinen, H.; Jaakkola, A.; Guan, F.; et al. Terrestrial Laser Scanning in Forest Inventories. *ISPRS J. Photogramm. Remote Sens.* **2016**, *115*, 63–77. [CrossRef]

55. Hyyppä, J.; Hyyppä, H.; Leckie, D.; Gougeon, F.; Yu, X.; Maltamo, M. Review of Methods of Small-footprint Airborne Laser Scanning for Extracting Forest Inventory Data in Boreal Forests. *Int. J. Remote Sens.* **2008**, *29*, 1339–1366. [CrossRef]

56. Gonçalves-Seco, L.; González-Ferreiro, E.; Diéguez-Aranda, U.; Fraga-Bugallo, B.; Crecente, R.; Miranda, D. Assessing the Attributes of High-Density Eucalyptus Globulus Stands Using Airborne Laser Scanner Data. *Int. J. Remote Sens.* **2011**, *32*, 9821–9841. [CrossRef]

57. Roussel, J.-R.; Caspersen, J.; Béland, M.; Thomas, S.; Achim, A. Removing Bias from LiDAR-Based Estimates of Canopy Height: Accounting for the Effects of Pulse Density and Footprint Size. *Remote Sens. Environ.* **2017**, *198*, 1–16. [CrossRef]

58. Comesaña-Cebral, L.; Martínez-Sánchez, J.; Lorenzo, H.; Arias, P. Individual Tree Segmentation Method Based on Mobile Backpack LiDAR Point Clouds. *Sensors* **2021**, *21*, 6007. [CrossRef] [PubMed]

59. Seidel, D.; Ammer, C. Efficient Measurements of Basal Area in Short Rotation Forests Based on Terrestrial Laser Scanning under Special Consideration of Shadowing. *IForest—Biogeosci. For.* **2014**, *7*, 227–232. [CrossRef]

60. Guerra-Hernández, J.; Arellano-Pérez, S.; González-Ferreiro, E.; Pascual, A.; Sandoval Altelarrea, V.; Ruiz-González, A.D.; Álvarez-González, J.G. Developing a Site Index Model for P. Pinaster Stands in NW Spain by Combining Bi-Temporal ALS Data and Environmental Data. *For. Ecol. Manag.* **2021**, *481*, 118690. [CrossRef]
61. Pascual, A. Building Pareto Frontiers under Tree-Level Forest Planning Using Airborne Laser Scanning, Growth Models and Spatial Optimization. *For. Policy Econ.* **2021**, *128*, 102475. [CrossRef]
62. Cabo, C.; Del Pozo, S.; Rodríguez-Gonzálvez, P.; Ordóñez, C.; González-Aguilera, D. Comparing Terrestrial Laser Scanning (TLS) and Wearable Laser Scanning (WLS) for Individual Tree Modeling at Plot Level. *Remote Sens.* **2018**, *10*, 540. [CrossRef]